Atmos. Meas. Tech. Discuss., 6, 7251–7313, 2013
www.atmos-meas-tech-discuss.net/6/7251/2013/
doi:10.5194/amtd-6-7251-2013

Atmospheric Measurement Techniques Discussions

Observing wind, aerosol particles, cloud and precipitation: Finland's new ground-based remote-sensing network

A. Hirsikko[1,2], E. J. O'Connor[1,3], M. Komppula[4], K. Korhonen[4], A. Pfüller[4], E. Giannakaki[4], C. R. Wood[1], M. Bauer-Pfundstein[5], A. Poikonen[1], T. Karppinen[6], H. Lonka[1], M. Kurri[1], J. Heinonen[1], D. Moisseev[7], E. Asmi[1], V. Aaltonen[1], A. Nordbo[7], E. Rodriguez[1], H. Lihavainen[1], A. Laaksonen[1], K. E. J. Lehtinen[4,8], T. Laurila[1], T. Petäjä[9], M. Kulmala[9], and Y. Viisanen[1]

[1]Finnish Meteorological Institute, P.O. BOX 503, 00101, Helsinki, Finland
[2]Forschungszentrum Jülich GmbH, Institut für Energie-und Klimaforschung: Troposphäre (IEK-8), Jülich, Germany
[3]Meteorology Department, University of Reading, Reading, UK
[4]Finnish Meteorological Institute, P.O. Box 1627, 70211, Kuopio, Finland
[5]Meteorologische Messtechnik GmbH (METEK), Elmshorn, Germany
[6]Finnish Meteorological Institute, Tähteläntie 62, 99600 Sodankylä, Finland
[7]Dept. of Physics, University of Helsinki, P.O. BOX 48, 00014 Univ. of Helsinki, Helsinki, Finland
[8]University of Eastern Finland, Dept. Applied Physics, POB 1627, 70211 Kuopio, Finland

[9]Dept. of Physics, University of Helsinki, P.O. BOX 64, 00014 Univ. of Helsinki, Helsinki, Finland

Received: 27 June 2013 – Accepted: 22 July 2013 – Published: 8 August 2013

Correspondence to: A. Hirsikko (anne.hirsikko@fmi.fi, a.hirsikko@fz-juelich.de)

Published by Copernicus Publications on behalf of the European Geosciences Union.

Abstract

The Finnish Meteorological Institute, in collaboration with the University of Helsinki, has established a new ground-based remote-sensing network in Finland. The network consists of five topographically, ecologically and climatically different sites distributed from southern to northern Finland. The main goal of the network is to monitor air pollution and boundary layer properties in near real time, with a Doppler lidar and ceilometer at each site. In addition to these operational tasks, two sites are members of the Aerosols, Clouds, and Trace gases Research InfraStructure Network (ACTRIS); a K_a-band Doppler cloud radar at Sodankylä will provide cloud retrievals within CloudNet, and a multi-wavelength Raman lidar, POLLY^{XT} (POrtabLe Lidar sYstem eXTended), in Kuopio provides optical and microphysical aerosol properties through EARLINET (European Aerosol Research Lidar Network to Establish an Aerosol Climatology). Three C-band weather radars are located in the Helsinki metropolitan area and are deployed for operational and research applications. We carried out two inter-comparison campaigns to investigate the Doppler lidar performance. The aims of the campaigns were to compare the backscatter coefficient and retrieved wind profiles, and to optimise the lidar sensitivity through adjusting the telescope focus and data-integration time to ensure enough signals in low-aerosol-content environments. The wind profiles showed good agreement between different lidars. However, due to inaccurate telescope focus setting and varying receiver sensitivity, backscatter coefficient profiles showed disagreement between the lidars. Harsh Finnish winters could pose problems, but, due to the built-in heating systems, low ambient temperatures had no, or only a minor, impact on the lidar operation: including scanning-head motion. However, accumulation of snow and ice on the lens has been observed, which can lead to formation of a water/ice layer thus attenuating the signal inconsistently. Thus, care must be taken to ensure continuous snow removal.

AMTD
6, 7251–7313, 2013

1 Introduction

Polar areas have been observed to be especially vulnerable to climate change (ACIA, 2005; IPCC, 2007). Several factors influence global climate change. Clouds are a major component in the global hydrological cycle, for example by storing, transporting and redistributing water. Clouds also contribute to global energy balance through reflecting, transmitting and radiating solar energy. Cloud properties (e.g. albedo, precipitation rate and lifetime) depend, amongst other factors, on number concentration of aerosol particles and on their chemical composition (Twomey, 1974; Albrecht, 1989; Lohmann and Feichter, 2005). Despite intensive research, interaction between aerosol particles and clouds is still one of the least-understood elements of Earth's climate (McFiggans et al., 2006), with uncertainty arising from: (i) environment-dependent sources of primary and secondary particles, (ii) varying spatial and temporal distribution and composition of aerosol particles, (iii) cloud and below-cloud dynamics, microphysics and precipitation (e.g. Chen and Penner, 2005; Hegg et al., 2012; Makkonen et al., 2012). In addition to indirect climate effects, aerosol particles have hazardous health effects and direct atmospheric radiative impacts (Haywood and Boucher, 2000; IPCC, 2007; Myhre, 2009). There is a sensitive balance between certain factors cooling and other factors warming the climate. Assessment of these factors contributing to climate change requires careful research at the process level in order to implement suitable parameterizations in global-scale models (IPCC, 2007; Lohmann et al., 2010).

Clouds, and their interaction with the environment, have been investigated through in-situ airborne measurements (e.g. Heymsfield, 2002), ground based campaigns (e.g. Verheggen et al., 2007; Lihavainen et al., 2010; Kamphus et al., 2010) or continuous observations (e.g. Marinoni et al., 2004; Portin et al., 2009). In-situ observations provide information at the process level; however, airborne measurements are expensive, and thus the number of observations is limited. In-situ ground-based observations require cloud base to be low enough for the station to be inside the cloud. Both of these methods lack the columnar information on cloud layers, their dynamics and optical

AMTD
6, 7251–7313, 2013

properties. Satellite and ground-based remote-sensing techniques have been developed for cloud-profile investigation. Synergy of light/radio detecting and ranging (i.e. lidar, ceilometer and radar) techniques has provided breakthroughs for cloud dynamical and microphysical research at fine temporal and spatial resolution (e.g. O'Connor, 2005; Westbrook et al., 2010a,b). Ideally, a combination of in-situ and remote-sensing observations would provide the best basis for process-level research of clouds. Assessment of cloud-profile climatology from satellite (Delanoë et al., 2011) and ground-based active instrumentation (Illingworth et al., 2007) is useful for global climate modelling. However, despite the development of instrumentation and data-analysis techniques, an understanding of the full coupling between cloud processes and their subsequent feedback mechanisms is still required (Bony et al., 2006).

With regard to aerosol particles, their emission rates, the quantity and quality of sources, distribution within the atmospheric boundary layer (ABL) and subsequent entrainment into the free troposphere: all have an effect on atmospheric radiative properties and air quality. Forest fires emit aerosol particles with strong climate and health impacts, and volcanic eruptions are hazardous for aviation with an immediate impact on the economy, and hence, for such events, real-time knowledge of the transport, dispersion and extent of the ash plume in the atmosphere is crucial. During the Iceland volcanic eruptions in 2010, research institutes in some European countries were well prepared to monitor ash plumes in the troposphere (e.g. Ansmann et al., 2011; Sicard et al., 2012; Rolf et al., 2012; Pappalardo et al., 2013). Ash layers were detected, and particularly well identified with lidars with depolarisation capability. In Finland, only a short observation period with a Raman lidar was possible in Helsinki, from which it was possible to identify the ash plume from Grimsvötn volcano as it passed over Finland in the spring of 2011. Despite the lack of comprehensive remote-sensing observations, balloon-borne in-situ measurements were performed in order to characterise the volcanic ash particulate properties (Petäjä et al., 2012). Experimental investigation of aerosol-particle climatology requires columnar information of aerosol-particle properties, which can be collected with satellite-based and ground-based active and passive

AMTD
6, 7251–7313, 2013

remote-sensing sensors (Remer et al., 2005; Sundström et al., 2009; Aaltonen et al., 2012; Kolmonen et al., 2013).

Turbulent atmospheric mixing transports gases and aerosol particles of biogenic and anthropogenic origin both within the ABL, and into the free troposphere (Barlow et al., 2011), and thus, can have an impact on air quality and process, like secondary particle formation (e.g. Janssen et al., 2012; Hirsikko et al., 2013), taking place in atmospheric. The ABL is also influenced by local topography (e.g. Barlow and Coceal, 2009; Collier et al., 2010). The urban environment is typically composed of roughness elements (buildings and trees) with different heights creating temporally and spatially varying wind and turbulent fields (Wood et al., 2009a); waves and trees induce a similar effect above the ocean and forest, respectively. Thus, characterising the effect of surface topography and roughness is essential in order to understand the nature of the ABL and processes taking place therein. In addition, buildings and streets enable turbulent mixing in the urban environment even when the rural surrounds are expected to be quiescent such as during night time (Souch and Grimmond, 2006), and temperature contrasts in coastal areas due to the ocean heat storage, generate sea/land breezes (e.g. Gahmberg et al., 2010). Thus, understanding ABL evolution and dynamics in different environments is essential in terms of air quality, climate-change assessment and weather forecasting.

The ABL has traditionally been monitored with instruments mounted on low-level (less than 100 m-tall) masts, and associated modelling (van Ulden and Wieringa, 1996; Barlow and Coceal, 2009). Although mast measurements have proven to be valuable for surface-layer meteorological research, mast-based experimental information on ABL evolution is largely missing. However, deployment of sodars and Doppler lidars enables the investigation of ABL wind (e.g. Wood et al., 2009b, 2013a,b), and its turbulent nature from high-resolution vertical velocity profiles (e.g. Hogan et al., 2009; O'Connor et al., 2010; Barlow et al., 2011).

Intensive remote-sensing instrument stations and networks for profiling of the ABL – and tropospheric aerosol particle, cloud and precipitation – have been established

AMTD
6, 7251–7313, 2013

by national research and weather service institutes, and in international collaborations (e.g. Illingworth et al., 2007; Flentje et al., 2010; Madonna et al., 2011; Shupe et al., 2013). Previously, a long-term program, the Helsinki Testbed, was implemented for testing and improving various instruments for weather monitoring and research purposes (Koskinen et al., 2011). Recently, the Finnish Meteorological Institute (FMI), together with the University of Helsinki (UHEL), has established Finland's new ground-based remote-sensing network (the present paper). The network covers five climatically, environmentally and topographically different locations across Finland, with the aims to: (1) provide near-real-time information on the distribution of aerosol particles and wind profiles in the ABL for stakeholders such as in now-casting, public information and for the aviation-safety authority; (2) estimate ABL depths; (3) investigate aerosol particles, clouds and precipitation to understand climate interaction; and (4) facilitate interdisciplinary research between atmospheric and ecological sciences.

In this paper, we introduce Finland's ground-based remote-sensing network, the instrumentation deployed, potential of the selected instruments and the measurement strategy at each location. In addition, we focus on the performance of Doppler lidars in challenging environments, by presenting results from two Doppler lidar intercomparison campaigns performed in Helsinki and discussing the lidars' operational reliability.

2 Measurement sites

Finland's ground-based remote-sensing network consists of five measurement stations (Fig. 1), which represent a variety of climates, and geological and topographical environments (full details given in Table 1):

1. Helsinki – an urban station (Sect. 2.1),
2. Kuopio – semi-urban/rural (Sect. 2.2),
3. Hyytiälä – rural (boreal forest) (Sect. 2.3),

AMTD
6, 7251–7313, 2013

4. Sodankylä – arctic rural (Sect. 2.4),

5. Utö – an island in Finnish archipelago (Sect. 2.5).

A four-season climate with a harsh winter is common for all stations; average wintertime snow depth is 5–20 cm on the southern coast and up to 80 cm in eastern and northern Finland. The measurement stations have a long tradition in atmospheric ground-based passive remote sensing and in-situ observations (Hari and Kulmala, 2005; Engler et al., 2007; Järvi et al., 2009; Leskinen et al., 2009).

2.1 Helsinki

Helsinki, the capital of Finland, is situated on the coast of the Baltic Sea, and is populated with over 1 million inhabitants in the metropolitan area. The coastline is ragged and numerous islands are close to the shore, and the city centre is next to shore. The proportion of forest and park areas increases with distance from the city centre of Helsinki. There are numerous weather and air quality monitoring stations in Helsinki and the surrounding metropolitan area (http://ilmatieteenlaitos.fi/suomen-havainnot/asema?parameter=4&station=101004; http://www.hsy.fi/en/Pages/Default.aspx). The majority of the research-based atmosphere measurements take place on the Kumpula campus of the FMI and the UHEL, 4–5 km north-east from the city centre. The campus is surrounded by forest and buildings to the west and north, and by park, buildings and sea to the east and south. A detailed overview of the surroundings and operation of the Station for Measuring Ecosystem–Atmosphere Relations III (SMEAR III, http://www.atm.helsinki.fi/SMEAR/) at Kumpula is given by Järvi et al. (2009). The station provides continuous measurements of meteorological quantities (e.g. temperature, radiation, wind speed and direction, precipitation), aerosol particle characterisation, various trace gas concentrations and eddy-covariance fluxes (Järvi et al., 2009a, 2012; Nordbo et al., 2012). In addition, an Aerosol Robotic Network (AERONET; Holben et al., 1998) Cimel sun photometer (at 52.8 m a.s.l.), Vaisala ceilometer CL31

AMTD
6, 7251–7313, 2013

and HALO Photonics Streamline Doppler lidar operate on the roof of the FMI building (44.4 m a.s.l.).

The Doppler lidar is also part of a comprehensive meteorological measurement network, Helsinki URban Boundary-layer Atmosphere Network (Helsinki URBAN Wood et al., 2013b). The main aim of Helsinki URBAN is to understand urban meteorological phenomena (Wood, 2010) with the help of continuous measurements from remote sensing (e.g. sodar, scintillometer, Doppler lidar) and in-situ instruments.

In addition, the FMI (and Aalto University) have the capability for airborne in-situ observations with a Skyvan airplane, as well as Cessna 172 capable of observing the atmospheric aerosol particles (Schobesberger et al., 2013) in collaboration with University of Helsinki, for which regular annual flight campaigns are performed.

2.2 Kuopio

Kuopio is a town with ca. 100 000 inhabitants located in eastern Finland and surrounded by lakes and forests. Remote sensing and in-situ measurements are distributed across three locations in Kuopio (Fig. 1):

- Vehmasmäki – rural forest area 18 km from the town centre of Kuopio;
- Savilahti – University of Eastern Finland campus, semi-urban environment;
- Puijo tower – observation tower on a hill covered by coniferous forest.

The multi-wavelength lidar POLLY^{XT} – POrtabLe Lidar sYstem eXTended (see Sect. 3.2) has been deployed continuously at the Vehmasmäki site since November 2012. There is a mast (300 m tall) in the immediate vicinity providing temperature, humidity and wind measurements at numerous levels up to the top. Ground-level aerosol-particle measurements at Vehmasmäki include aerosol particle total scatter and backscatter (nephelometer), aerosol absorption/BC (aethalometer) and particle mass.

AMTD
6, 7251–7313, 2013

These measurements are supported by two nearby sites, Savilahti and Puijo tower (SMEAR IV) which are both about 3 km from Kuopio town centre and 2 km separate from each other. The SMEAR IV belongs also to the Integrated Carbon Observation System (ICOS, http://www.icos-infrastructure.fi/) network concentrated on measurements of greenhouse gas concentrations and meteorological quantities. The campus at Savilahti hosts the FMI Kuopio unit in the Melania building, on the roof of which several instruments are installed: a Doppler lidar (HALO Photonics), instruments for measuring aerosol optical thickness (AERONET Cimel sun photometer) and solar irradiance (direct, diffuse and global; a pyranometer and a multi-filter rotating shadow band radiometer). A Vaisala CT25K ceilometer and automatic weather station are located on the ground within 20 m of the building.

The top of Puijo tower is 224 m above lake level (i.e. 306 m a.s.l.), on which instrumentation for aerosol-particle size distribution and optical property characterisation is installed (Leskinen et al., 2009, 2012). Every autumn, a cloud-measurement campaign is conducted at Puijo, since the hill and tower are often inside clouds. The Doppler lidar at Savilahti has the potential for direct line-of-sight scanning above the Puijo tower.

2.3 Hyytiälä

SMEAR II station is in a homogeneous coniferous forest at Hyytiälä. The area around the measurement station is sparsely populated and land use is dominated by forestry and agriculture. Hyytiälä is about 60 km from the nearest town, Tampere (ca. 210 000 inhabitants in 2012). The UHEL-operated station has a long tradition in ground-based in-situ measurements (Hari and Kulmala, 2005). The measurement station, its operation and surroundings were introduced in detail by Vesala et al. (1998); therefore, we give only a short description of the current status here.

The measurements include continuous observations of meteorological quantities (e.g. temperature, cloud base height, wind speed and direction), comprehensive aerosol particle physical, optical and chemical properties, trace gas concentrations, gas exchange, water and energy balance (e.g. Manninen et al., 2009; Ilvesniemi et al.,

AMTD
6, 7251–7313, 2013

2009, 2010; Launiainen, 2010; Laitinen et al., 2011). Furthermore, measurements are operated in soil, inside and above forest canopy, above the nearby lake Kuivajärvi and Siikaneva wetland. Every spring – during intensive field campaigns – extensive aerosol particle, trace gas and ion measurements are performed (e.g. Kulmala et al., 2007; Williams et al., 2011). Aerosol optical depth is monitored by the Cimel and total ozone column with Brewer MK III spectrometer. The SMEAR II station provides data through AERONET, ICOS, Aerosols, Clouds, and Trace gases Research InfraStructure Network (ACTRIS), Analysis and Experimentation of Ecosystems (ANAEE) and Integrated non-CO_2 Greenhouse gas Observing System (INGOS).

A Doppler lidar (HALO Photonics) was placed on a roof (of the maintenance building) in December 2012, 400 m from the main measurement area where the Vaisala ceilometer is also located. The current location of the Doppler lidar was selected based on the criteria of a stable base, and a clear view for wind profiling and horizontal scanning. In the future, it is possible that the Doppler lidar will be moved closer to the other measurements when the construction of a new sturdy tower has been completed.

2.4 Sodankylä

The Arctic Research Centre (ARC, http://fmiarc.fmi.fi; Kivi et al., 1999) of the FMI is located 7 km from the centre of the town Sodankylä (5500 inhabitants) and is situated north of the Arctic circle (Fig. 1). The centre has been constructed on the bank of the river Kitinen and is surrounded by coniferous forest dominated by pine trees. Much of the land nearby is a large bog. An infrequently operated airport (light aircraft, gliders and helicopters) is located 4 km north of the ARC.

A Doppler cloud radar (Metek GmbH) has been installed close to the radiosounding station and next to MARL (Mobile Aerosol Raman Lidar) of the Alfred Wegener Institute for Polar and Marine Research, Germany (AWI), Germany. Manual balloon-borne soundings of ozone are performed weekly at the sounding station, together with other less-frequent special soundings including water vapour and aerosol particle properties. Radiosoundings for vertical profiles of meteorological quantities are carried out twice

AMTD
6, 7251–7313, 2013

a day by a Vaisala Automatic Sounding Station. In addition to that, the site also gathers automatic synoptic weather observations. The sounding-station roof and a 16 m tower beside it accommodate a Vaisala CT25K ceilometer, Doppler lidar (HALO Photonics) and radiation sensors (including spectral measurements in the UV-range, global, reflected, diffuse and direct components of solar radiation). Total ozone column is measured with a Brewer MK III spectrometer, aerosol optical depth is observed with Precision Filter Radiometer (PFR) and CO_2 and CH_4 columns are measured with Fourier Transform Spectrometer. A recent investment was made in a Cimel instrument with additional cloud mode feature which enables investigation of cloud optical properties through AERONET (Chiu et al., 2010).

There is a meteorological mast 500 m south of the sounding station, providing temperature, humidity and wind speed at 3, 8, 18, 32, 45 and 48 m. Surface-layer turbulence is estimated with sonic-anemometer eddy-covariance measurements at heights of 25 and 48 m. Fluxes of water vapour and carbon dioxide are calculated from CO_2/H_2O Gas Analysers which are co-located with the sonic anemometer. Snow depth, soil temperature and soil respiration measurements are carried out next to the mast.

2.5 Utö

The island of Utö (Fig. 1) is on the outer edge of the Finnish archipelago in the Baltic Sea, 60 km southwest from the mainland and about 10 km from the next nearest island of similar or larger size. The 1 km^2 island is a background site whose air quality is influenced regularly by nearby ship traffic (Hyvärinen et al., 2008). The sea around Utö is ice-free almost year-round except in the direction of the archipelago (north), which can be covered by ice for one or two months. The ground is rocky and partly covered by underbrush. The island has about 50 yr-round inhabitants.

The FMI performs a wide range of atmospheric observations in Utö. Due to its location beside the main ship tracks, monitoring of the weather has a long tradition on the island. These observations include temperature, wind speed, direction, visibility

AMTD
6, 7251–7313, 2013

and cloud-base height. Engler et al. (2007) introduced continuous ground-based in-situ aerosol-particle observations in 2003. In addition, Utö is a member of the ICOS network. Measurements within ICOS include monitoring of greenhouse gas concentrations and meteorological quantities. Recent investments at Utö include a Doppler lidar (HALO Photonics) and a comprehensive sea gas flux and wave observation station. The greenhouse-gas-monitoring station operates on the northern side of the island (Enskär). Sea gas flux and wave measurements are carried out west of cape Kesnäs, and aerosol particulate, Doppler lidar, ceilometer and other operational weather observations are made on the eastern side of the island (Österäng). The Doppler lidar is placed on top of an old measurement container (ca. 8 m a.s.l.) and has an almost uninterrupted view down to low elevations in every direction except for the lighthouse on the island in north-west direction.

3 Instrumentation

The building of Finland's ground-based remote-sensing network has been made step-by-step (Table 1): (1) deploying the Helsinki weather radar network, which is a joint co-operation between the FMI, the UHEL and Vaisala Inc., (2) utilising the existing ceilometer network and starting backscatter-profile collection in Helsinki, Kuopio, Hyytiälä and Sodankylä in 2009, (3) installing three Streamline Doppler lidars in 2011, (4) installing a scanning Doppler cloud radar and two Doppler lidars in 2012 and 2013, and (5) starting ceilometer backscatter-signal collection in Utö in the future. In addition, one spare Doppler lidar was purchased: in order to replace one of the network lidars in the case of malfunction (in between times, various research campaigns are planned for the spare lidar). In the following we give a description of the each remote-sensing instrument (Table 2).

AMTD
6, 7251–7313, 2013

3.1 Doppler lidar

The FMI has five network, and one spare, pulsed Doppler lidars from HALO Photonics (http://halo-photonics.com/, Pearson et al., 2009). The backscatter return of the pulsed 1.5 µm wavelength signal is observed with a heterodyne detector (Table S1, Supplement). The Doppler lidar measures scattered signal in co- and cross channels which allows determination of the depolarisation ratio of scattering targets. Doppler lidars are equipped with built-in heating and cooling systems. In addition, the lidar lens and calibration plate are heated to try to avoid snow gathering and ice formation.

The FMI has two types of Doppler lidars (four Streamline and two Streamline Pro model lidars), whose characteristics are identical apart from scanning capabilities and receiver sensitivity. The Streamline model Doppler lidars are capable of full hemispheric scanning. The recent Streamline Pro model lidars have no external moving parts, since the scanning head is mounted inside the lidar case. However, only limited range (±20° around zenith) scanning with 360° azimuth range is possible. According to the manufacturer the Pro model has a narrower receiver frequency bandwidth and therefore it should be more sensitive, which makes it more suitable for arctic conditions.

The time resolution can be as fast as 5 s, which includes 1 s of measurement and then data processing and storing. However, to allow long enough data collection, and thus to obtain good data quality, our integration resolution has been 20–30 s. The spatial resolution of Doppler lidar aerosol particle return is vertically limited to the height of higher aerosol load (almost always only in the ABL) and nearly horizontally to a varying maximum of about 0.5–4 km. Water, mixed phase and ice clouds can be detected out to the maximum 9.6 km detection range.

Continuous vertical staring and a Doppler Beam Swinging (DBS) wind profile measurement every ten minutes are standard operation modes for the FMI Doppler lidars. In between the operational tasks, custom-designed scanning is performed. Until now various vertical azimuth display (VAD) and range height indicator (RHI) strategies are

AMTD
6, 7251–7313, 2013

deployed in Utö (see Sect. 5.1) and Helsinki. Similar strategies are planned to be carried out in Hyytiälä and Kuopio, which have full hemispheric scanning lidars.

Standard Doppler lidar data includes the profiles of signal-to-noise ratio (SNR), uncelebrated backscatter coefficient (β) and Doppler velocity. The Doppler lidar backscatter coefficient is calibrated according to a procedure introduced by O'Connor et al. (2004). In this method integration of β from a nearly non-drizzling cloud base to infinity is set equal to $1/(2\eta S)$, where η is the multiple scattering factor and S is the lidar ratio. Both η (close to 1) and S (20 sr) are assumed constant and known for lidar wavelength in stratocumulus clouds. A non-drizzling condition 250 m below the cloud base is determined by requiring backscatter coefficient values to be smaller than certain threshold value, namely 10 times smaller than backscatter coefficient inside liquid cloud (O'Connor et al., 2004). We do not deploy any calibration procedure for depolarisation ratio or Doppler velocity. Wind profile data are measured using the DBS technique: where one vertical beam, one northward beam and one eastward beam are measured. Northward and eastwards beams are tilted 15–20° from zenith. Wind speed and direction are calculated using trigonometry and assuming that no major changes occur within the DBS volume (Lane et al., 2013). Custom scanning data require different methods to provide more sophisticated information (e.g. Banta et al., 2006; Wood et al., 2013a).

3.2 Raman lidar

The lidar at Vehmasmäki (62°44′17″ N, 27°32′33.5″ E, 190 m a.s.l.) is a seven-channel Raman lidar POLLY^{XT} (Table S2, Supplement; Althausen et al., 2009; Engelmann et al., 2012). The POLLY^{XT} provides vertical profiles of the particle backscatter coefficient at 355, 532 and 1064 nm, and the particle extinction coefficient at 355 and 532 nm. The Raman method (Ansmann et al., 1992) is deployed to estimate backscatter coefficients at 355 and 532 nm. The relative statistical error is typically < 5 % for the backscatter coefficients and < 10 % for the extinction coefficients. For the backscatter-coefficient profiles at 1064 nm and within the troposphere, the Klett method (Klett, 1981) is used

AMTD
6, 7251–7313, 2013

assuming height-constant lidar ratios. An overlap correction following Wandinger and Ansmann (2002) is deployed. We use threshold value 0.7 for the overlap correction which allows data starting from 500 m or even lower. Columnar aerosol optical depth can be estimated from the integrated extinction coefficients with the assumption of a constant extinction for the first 500 m. The vertical resolution is 30 m and currently we store the raw data in 30 s averages.

Intensive particle quantities such as the Ångström exponents, the lidar ratio at 355 and 532 nm and linear particle depolarization at 532 nm can be analysed. The top height and the evolution of the ABL and night-time residual layer can be defined together with the macro physical properties (i.e. height and thickness) of cloud and aerosol layers (Fig. 2). The depolarization channel (532 nm) allows separation of spherical and non-spherical targets. Thus, dust particles can be identified and the ratio of ice crystals and water droplets in clouds estimated. The system also includes a water–vapour channel (407 nm) (Engelmann, 2012). With the continuous measurement of aerosol particle backscatter, extinction, depolarization and water–vapour mixing ratio, the lidar is suitable for cirrus cloud and aerosol particle studies as well as for stratospheric observations during darkness.

In the example measured on 31 March 2013, two pronounced layers were identified. First the ABL evolution in the lowermost 2 km, where aerosol particles are well mixed, can be followed. Secondly the evolution of an elevated aerosol-particle layer was observed within the free troposphere, at around 7–8 km altitude (Fig. 2). Aerosol-particle depolarization ratio (Fig. 2) was rather low for this layer, and hence indicates the presence of spherical, i.e. more-aged or hydrophilic, particles. The water–vapour measurements showed enhanced relative humidity within the ABL, while the elevated aerosol-particle layer was drier. The example from 31 March 2013 shows, how the POLLY^{XT} Raman lidar can be used for tropospheric aerosol-particle studies of the ABL (Korhonen et al., 2013), the characterization of elevated tropospheric aerosol-particle layers (Giannakaki et al.: Optical and microphysical characterization of different aerosol types using multiwavelength lidar measurements in South Africa, in preparation, 2013a), for

AMTD
6, 7251–7313, 2013

water–vapour profiling and continuous long-term monitoring (Komppula et al., 2012; Giannakaki et al.: Long-term lidar observations of free tropospheric aerosols layers over South Africa, in preparation, 2013b). Compared to Doppler lidar, the POLLY^{XT} is more sensitive to elevated aerosol particle layers and the independent determination of backscatter and extinction profiles allows calculation of microphysical properties of aerosol particles when inversion methods are used (Althausen, 2009; Giannakaki et al., 2013a).

Microphysical data can be derived with inversion algorithms. By following the method developed at the Leibniz Institute for Tropospheric Research (Müller et al., 1999a,b) we can estimate values for the particle surface area, volume, effective radius, refractive index and single scattering albedo at 532 nm. Uncertainties in the retrievals are estimated according to Müller et al. (1999a,b). The uncertainty for effective radius is $< 30\,\%$ and for volume and surface area concentration $> 50\,\%$. The maximum uncertainty of real part of the complex refractive index is ± 0.1. When the imaginary part is > 0.01i the uncertainty can be as high as 50 %. The accuracy of single scattering albedo depends on uncertainties of the optical data.

POLLY^{XT} has been part of the European Aerosol Research Lidar Network (EARLINET; Bösenberg et al., 2003) since 2012. The objectives of EARLINET are reached by operating a network of, presently, 23 stations distributed over Europe using advanced quantitative laser remote sensing to directly measure the horizontal, vertical and temporal distribution of aerosol particles. Special care is taken to assure data quality, including instrument inter-comparison. A major part of the measurements is performed according to a fixed schedule to provide an unbiased and statistically significant dataset. Additional measurements are performed to specifically address temporally or spatially limited aerosol events.

The lidar is mounted in a container, which has a glass window on the top, in order to prevent hazardous effects of ambient temperature changes and snowfall. The operation of the Raman lidar is planned to be continuous in Vehmasmäki. However, in the case of

AMTD
6, 7251–7313, 2013

precipitation, the measurements are stopped automatically. The device is portable and it can be transported, e.g. in the case of a volcanic eruption, to detect aerosol plumes.

3.3 Doppler cloud radar

MIRA-35S (http://metekgmbh.dyndns.org) is a full-hemispheric scanning Doppler Cloud radar (Görsdorf et al., A 35 GHz radar for long term observations of cloud parameters – Description of system, data processing and sampling strategy, in preparation, 2013). In order to detect clouds, a high sensitivity is required. The reflectivity of visible clouds is in the range −70 to −20 dBZ, the reflectivity of rain droplets is in the range +15 to +60 dBZ; and the reflectivity of drizzle below clouds is in the reflectivity range between values from cloud and precipitation. The cloud radar is optimized to be sensitive to cloud and drizzle droplets at short range (up to 30 km) with fine spatial resolution (typically 30 m). For comparison, weather radars provide large range coverage (up to 150 km around the radar) with sufficient sensitivity for detecting rain (see Sect. 3.4). Compared to lidars, the extinction of the radar signal in non-precipitating clouds is negligible.

The Doppler cloud radar is based on a 35 GHz magnetron transmitter providing short pulses with high pulse power which allows a range resolution of 30 m and sufficient sensitivity for most of the visible clouds (see Table S3, Supplement, for technical details). Typically a pulse repetition frequency (PRF) of 5 kHz is used, which allows a maximum range of 30 km and a velocity range of $\pm 10.6\,\mathrm{m\,s^{-1}}$. The radar signal is converged by a Cassegrain-antenna having 1 m diameter and beam width of 3 dB. From the down-converted receiving signal of each range gate, Doppler spectra are calculated using a 512 point Fast Fourier Transform (FFT). One profile of spectra is calculated from the signal of 512 successive pulse cycles (0.1024 s). Typically 100 spectra (10 s) are averaged to increase the statistical significance and sensitivity of the Doppler spectra. After removing the receiver noise from the averaged spectra, the first three moments (reflectivity, Doppler velocity and Doppler spectrum width) are calculated from the peaks identified in the spectra. The Doppler cloud radar transmits using vertical polarisation

AMTD
6, 7251–7313, 2013

(if the beam is pointing horizontally), and simultaneously receives in both the vertical and horizontal polarisation channels, hence providing linear depolarisation ratio (LDR).

The system can save raw data or un-averaged spectra, but normally only 10 s-averaged spectra are saved (30 GB day^{-1}). The spectra are routinely converted to a compressed format, thus saving only the spectral bins containing signal. Depending on the amount of clouds, these files typically occupy about 100 MB day^{-1}. The measurement strategy of the Doppler radar has been to point vertically and gather good quality data within 14 km.

Insects cause strong signals in the ABL. These signals can be recognized because they have high LDR values and because they are below the melting layer where the hydrometeors have very low LDR values. These signals are filtered in the way that for each range gate, one set of moments for the insects and one for the hydrometeors are saved.

3.4 Helsinki weather radar network

The Helsinki metropolitan area hosts three dual-polarized C-band weather radars. One of them, Vantaa weather radar (VAN), belongs to the FMI and is deployed for operational applications (Saltikoff and Nevvonen, 2011). The Kumpula Radar is located in Kumpula campus of the UHEL and is operated by the Department of Physics. The third radar is a research and development radar of Vaisala Inc. and is used for research purposes by the UHEL radar meteorology group. The Helsinki weather radar network is deployed to study high-latitude precipitation and its impact on quantity and quality of storm water, and it acts as one of ground validation sites for the upcoming NASA Global Precipitation Mission (Hou et al., 2008).

The current operations strategy includes synchronized scans at low elevation angles. Since the Vantaa radar operations schedule is fixed, Kumpula and Kerava radars perform low elevation scans with similar system setting to those of Vantaa radar every 15 min. An example of a joint retrieval is presented in Fig. 3, where snowfall rate is estimated by using the FMI operational snowfall-rate reflectivity relation (Saltikoff et al.,

AMTD
6, 7251–7313, 2013

2010) that was applied to the three-radar maximum-reflectivity composite. In Fig. 3b and c dual-Doppler wind speed and direction calculated from Doppler velocity measurements are shown.

Given the greater flexibility of the research radars, their operations schedule is adopted to current research interests. Juga et al. (2012) have presented the use of Vantaa and Kumpula radar observations to analyse the cause of a large traffic accident. In that study, Vantaa radar observations were supplemented by the vertical scans of Kumpula radar that provided a vertical structure of the precipitation field. The investigations, however, are not limited to pure meteorological applications. For example, Leskinen et al. (2011) have reported application of the radar observations to monitoring of pest insect immigration.

One of the current plans related to the Helsinki radar network is to upgrade it to distributed collaborative adaptive sensing (DCAS) capabilities (McLaughlin et al., 2009). This will be achieved by adding a fourth radar, which together with Kumpula and Kerava radars will form a DCAS network, where scanning strategies will be adaptively modified depending on weather conditions.

3.5 Ancillary remote-sensing observations

Ancillary remote-sensing instrumentation includes a Vaisala 905 nm wavelength ceilometer at each station (Vaisala, 1999). Traditionally, the ceilometer network has been utilized for cloud-base detection and cloud-cover monitoring in Finland. Furthermore, the ceilometers have collected aerosol-particle backscatter profiles in Sodankylä, Kuopio, Helsinki and Hyytiälä since 2009 (Table 1). Aerosol-particle profiles have traditionally been deployed to investigate ABL evolution (e.g. Millroy et al., 2011). Each station, excluding Utö, has a Cimel or Precision Filter Radiometer sun photometer to monitor columnar aerosol optical properties (Aaltonen et al., 2012). We have installed a new Cimel instrument with additional cloud optical-depth mode (Chiu et al., 2010) at Sodankylä in March 2013.

AMTD
6, 7251–7313, 2013

In Sodankylä, a 7-channel Raman lidar MARL (Immler et al., 2008), which is used to retrieve vertical profiles of cloud and aerosol-particle properties, as well as water–vapour profiles, is operated in the close proximity of the sounding station. MARL was installed in Sodankylä in September 2010. Since then the instrument has been operated by the FMI in cooperation with the AWI. The instrument was built in 1996 and it is owned by the AWI. It measures backscatter coefficient (co- and cross-polarized) and extinction coefficients at 355 and 532 nm, and water–vapour mixing ratio. It is very-well situated for higher tropospheric and stratospheric profiling.

Since January 2013 two Microwave (Radiometer Physics GmbH) radiometers have provided atmospheric brightness temperature. Sodrad1 (RPG-8CH-DP) measures at 10.65, 18.7, 21, 37 GHz and Sodrad2 (RPG-2CH-DP) measures at 90 and 150 GHz (Rose and Czekala, 2009). A scanning routine with 20 s integration in each direction has continuously been applied. By combining microwave radiometer, ceilometer, cloud radar, CloudNet (A network of stations for the continuous evaluation of cloud and aerosol profiles in operational NWP models) type data products (Illingworth et al., 2007) can be retrieved within the ACTRIS framework. The retrieval procedure provides cloud macro-physical and micro-physical properties.

4 Doppler-lidar performance

In Sect. 4.1 Doppler lidar operational reliability and challenges in Finland are discussed. In addition, results are introduced from two Doppler lidar inter-comparison campaigns which were carried out in Helsinki after the instruments had arrived from manufacturer (Sect. 4.2). The aim was to investigate performance and comparability of Doppler lidar wind and backscatter coefficient profiles. Comparability of instruments is essential because they were distributed to the network sites after the test periods. In Sect. 4.3 the Doppler lidar research applications potential for the network are introduced.

AMTD
6, 7251–7313, 2013

4.1 Doppler-lidar operation reliability and limitations in Finland

4.1.1 Observation limitations due to ambient conditions

The Doppler-lidar backscatter coefficient is proportional to $\sim nd^2$, i.e. target number concentration (n) and surface area where d is diameter (Weitkamp, 2005). Particles larger than $0.1\,\lambda$ in diameter, where λ is the scattered wavelength, scatter light according to Mie theory. Thus, Doppler lidar signal return is dominated by particles larger than 150 nm in diameter, while backscatter from air molecules is negligible.

Ambient aerosol-particle number concentration and mass is low or moderate at the network stations (e.g. Kulmala et al., 2001; Engler et al., 2007; Dal Maso et al., 2008; Leskinen et al., 2009), apart from Helsinki (Aarnio et al., 2005; Hussein et al., 2007). Therefore, it became quickly clear that special attention would be required for the setting up of measurements: since recording values lower than SNR were frequent and vertical length of line-of-sight was often only couple of hundred meters. Changing the telescope focus down to 1–2 km has helped us to collect more representative data higher in the ABL, as one could expect (Fig. S1, Supplement). The best response within the ABL is gained when the telescope focus is set to 2 km. The Doppler lidars have built-in software-controllable motors to change telescope focus. The newest Doppler lidars (one Streamline and both Steamline Pro models) have a software update, which enables adjustment of the telescope focus separately for each task, e.g. vertical stare and horizontal scanning. We consider that there is no universally optimal telescope focus setting for these Doppler lidars, but it rather depends on measurement environment and purpose of observations. We are interested in representative ABL observations in environments having low aerosol particle concentration, and therefore, short focus length is optimal within the Finnish network.

Changing the telescope focus is not always sufficient. To increase data acquisition sensitivity, the data integration time was increased from the minimum one ray per point to 4–6 rays per point depending on the site, where temporal resolutions are 5 and 20–30 s, respectively. This appeared to help to collect data higher from ABL aerosol

AMTD
6, 7251–7313, 2013

particles. At the beginning, a running integration of observed profiles was tested to gain high resolution (e.g. 10–12 s) data, and thus, with the help of the measurement software averaged different number of pulses (e.g. 150 000 or 450 000 per ray) at the background. However, it is possible that the computer was too occupied by multiple tasks that it was not capable of doing full integration as intended.

Despite the above-mentioned attempts, there still exists time periods of too low signal return from aerosol particles, even if the measurement was not affected by precipitation. This is especially a problem in the cross channel, since the signal of the channel from the moist ABL is often too low to allow for the calculation of the depolarisation ratio for aerosol particles. It remains a future task to further improve data quality with novel data-analysis methods.

Additionally, the detection range of ABL wind profiles derived from DBS data measured in Kuopio during one year (20 September 2011–20 September 2012) was analysed. Based on 23 092 wind-profiles observed during cloud-free conditions, the maximum detection range was 2340 m a.g.l. and the average range was 400 m (±1 standard deviation 250 m) a.g.l. The near-horizontal detection range has been checked in Helsinki and Utö, where good quality SNR-threshold-cleaned data have been collected up to 4.5 and 1.5 km, respectively. It is clear that, during rain or snow, the lidar signal is attenuated and the penetration distance depends on the amount of precipitation.

4.1.2 Effect of temperature and weather

The FMI operates the Doppler lidars throughout the year within the network. Thus, reliable operation in all weather conditions is preferable. Winter weather often sets special requirements for measurement devices. The Doppler lidar performance has been tested in a cold room at temperatures down to −20 °C by the manufacturer. The first harsh winter when the Streamline lidar was operated continuously was in Finland during winter 2011–2012, when ambient temperature decreased down to −26 °C. Based on experience of two winters, the operation of Doppler lidars was not affected by low ambient temperatures due to sufficient insulation of the system and a built-in heat-

AMTD
6, 7251–7313, 2013

ing system. The temperatures inside the instrument were always above 7 °C. Only the computer interface graphics were slower than usual.

However, accumulation of snow on top of the Doppler lidar may cause two kinds of problems. The first concern would be on the mobility of the scanning head when snow or ice accumulates on it. Based on experience, accumulation of a 30 cm of a soft snow layer does not cause problems for the mobility of the scanning head. However, formation of ice from melted snow or super cooled water has been observed to prevent mobility of the scanning head. On such occasions, the measurement software prevents control of the motors to prevent damage formation. The disadvantage is that measurements are still continued, and the scanning schedule tasks are apparently done. The second concern is related to accumulation of snow and ice on the lidar lens. Melting of snow into water attenuates the lidar signal (Fig. 4). The amount of signal attenuation depends on the water volume. Formation of thick snow and ice layers on the lens can attenuate the signal completely (Fig. 4). Thus, frequent maintenance is required in order to collect good-quality data continuously, since no measurement software provided warning flags are available.

The Streamline Pro lidar model was designed for arctic (i.e. low aerosol particle content) and harsh winter conditions. The new Pro model was tested in real winter conditions in Helsinki, Kuopio and Sodankylä for the first time during winter 2012–2013. With the help of an additional blower, the slanted window is kept relatively clean from water droplets and snow. However, manual cleaning is required during heavy snowfall.

4.2 Comparison of measurements

Data quality and reliability of measurement devices should be known and tested before beginning operational observations. Therefore, two inter-comparison measurement campaigns were conducted in Helsinki with the aim of comparing profiles of the backscatter coefficient, vertical velocity, horizontal wind speed and direction (Sects. 4.2.1–4.2.2). In addition, single range-gate wind velocity data were compared

AMTD
6, 7251–7313, 2013

against in-situ sonic anemometer data at SMEAR III station, and wind speed and direction observations at SMEAR IV (Sect. 4.2.3).

4.2.1 Measurement setup during inter-comparison campaigns

Intensive inter-comparison campaign was carried out by measuring with two or three Streamline Doppler lidars (production numbers 32–34) side-by-side on a concrete plate on the roof of the FMI in Helsinki (Table 3). The first inter-comparison campaign took place during autumn-winter 2011–2012. The campaign was carried out in two intervals (Table 3): (1) three or two lidars were side by side in September 2011, and (2) two lidars were ca. 100 m apart from each other starting in October 2011. During the measurements each lidar had a similar setup of telescope focus, data integration time, spatial (320 range gates with 30 m separation) and temporal (Table 3) resolution. Timing of wind profile or vertical stare measurements were not synchronized between Doppler lidars. A DBS scan was performed every 10 min and temporal resolution of vertical observations was 10 s during side-by-side comparison in September 2011. During the first inter-comparison campaign the lidars integrated vertical stare data and each of the tree DBS rays as a running mean over 10 and 30 s in the background by the measurement software during the first and second periods, respectively, while vertical data temporal resolution in the file was 10 s. During 10 s 150 000 pulses were averaged, while during 30 s 450 000 pulses were averaged. It is possible that averaging over 30 s sample was too large for the measurement computer to handle, while simultaneously collecting new data. Therefore, an unknown amount of data may have been excluded from each average. If this is the case, data of all lidars were equally affected, and thus, are comparable with each other. In the Sect. 4.2.2 we concentrate only on measurements with 10 s averaging.

The second inter-comparison campaign was carried out during winter 2012–2013 (Table 3). The two Streamline Pro model Doppler lidars (production numbers 53–54) measured next to a new Streamline lidar (no 46) on the roof of the FMI in Helsinki, and an old operational Streamline lidar (no 34) was measuring on the roof 100 m apart

AMTD
6, 7251–7313, 2013

from the other lidars. Deployed telescope focus and temporal resolution settings are presented in detail in Table 3. Doppler lidar spatial resolution was 320 range gates with 30 m separation. During the second campaign the possible mishandling of data by a running averaging was avoided. Data integration was increased by measuring 4–6 rays (15 000 pulses ray^{-1} ~ 5 s) per point. This decreases the temporal resolution of the data to 20–30 s. Wind profiles were collected every three minutes, while timing of DBS scans were not synchronised between lidars. In addition, the effect of the telescope focus length on data quality was investigated (see Table 3 for details). During the second campaign the measurements were hampered by nearly continuous rain and snow. Nonetheless, representative examples of liquid and ice cloud events could be found (Sect. 4.2.2).

4.2.2 Inter-comparison of backscatter coefficient and wind profiles

Backscatter coefficient profiles of (1) an aerosol particle layer, (2) a liquid cloud below and (3) above 1 km, and (4) ice clouds from cross- and co-channels were compared (Figs. 5 and 6). Each curve is a median over half an hour data centred on times indicated in Table 4. These case examples were considered representative in this qualitative analysis since they reflect general pattern observed during the inter-comparison periods. Comparisons of backscatter coefficients showed that some of the lidars provide comparable profiles, while clear differences in either both co- and cross-channels, or only on one of them, were also observed (Fig. 5). Differences are likely to arise from two reasons: (1) telescope focus was different from expected or (2) receiver sensitivity was low.

Examples from the first campaign indicate that the backscatter profiles of the co-channel measured with two lidars (production numbers 32 and 33) were comparable in all tested altitudes and from different targets. The third lidar (no 34) showed clearly higher values below 2 km in both channels. This indicates that the focus setting of lidar 34 was different than that of two other lidars, which was also supported, when a self-calibration procedure (O'Connor et al., 2004) was applied. Differences between

AMTD
6, 7251–7313, 2013

lidars 32 and 33 in the cross-channel are related to detection sensitivity. Detecting the different focus settings allows us to revise measurement software initial parameter file accordingly, and prevents misinterpretation of observations from different sites.

Backscatter profiles of two new lidars nos 46 (Streamline) and 53 (Streamline Pro) showed differences in the profiles compared to observations by the old lidar (no 34) and the third new lidar (no 54, Streamline Pro, Fig. 5). In the co-channel the lidar no 54 measured similar values below the 1 km liquid cloud and in the ice cloud as the focus shifted lidar no 34, but clearly higher values than the other two lidars. The aerosol return was comparable between lidar nos 34, 46 and 53, while lidar no 54 showed clearly higher backscatter coefficient values. The cross-channel profiles in the water cloud showed the opposite compared to co-channel, i.e. lidar no 54 measured smaller values. These results indicate different detection sensitivity between the instruments and polarity channels.

The second campaign was also intended to investigate the effect of the telescope focus position on uncertainty in backscatter profiles (Fig. 6). Changing the telescope focus to 1 or 2 km increased the detection efficiency in both liquid and ice clouds. Some increases in aerosol returns can also be observed when comparing the profiles of lidars nos 34 and 46. Unfortunately, these examples do not show how the detection sensitivity changes as a function of telescope focus position at higher altitudes above the lidar.

Wind velocity components were averaged over half an hour at each range gate and data from all available range gates are show in Figs. 7 and 8, and results of statistical comparison of these median data are shown in Table 5. In Fig. 7 we analysed measurement period 2–15 September 2011 and in Fig. 8 we analysed period 24 November–9 December 2012. During these periods each lidar had similar settings of telescope focus and data averaging time (Table 3). Comparison of wind velocity components, derived wind speed and direction showed generally good agreement between the instruments (Figs. 7 and 8, Table 5). Some deviation from the 1 : 1 line was evident and scattered points were observed. Each wind profile is a snapshot of a moment. Therefore, each single wind profile represents a slightly different atmospheric situation. As such, the

AMTD
6, 7251–7313, 2013

statistical sampling is relatively poor considering the turbulent nature of the ABL using the DBS method (Lane at el. 2013). So, despite averaging wind data over half an hour, small deviations around the 1 : 1 line were expected. During the second campaign, several days were affected by large amounts of snow which caused larger deviations of the compared wind quantities (Fig. 8, Table 5). The first measurement campaign was characterised by highly varying wind directions, which resulted in clearly scattered points, when wind direction measured by three lidars was compared (Fig. 7). When investigating profile by profile, these scattered points were observed at all heights. These results indicate also that the observed differences in receiver sensitivity and telescope focus do not affect wind observation accuracy, even though they affect the length of line-of-sight.

This was the first time that several identical Doppler lidars have been inter-compared to this level. Previously, vertical velocity and SNR profiles of two Streamline Doppler lidars have been inter-compered (Newson, 2012). Their results indicated reasonably good comparability of vertical velocity in the sufficient SNR range. SNR profile figures showed small differences in SNR intensity.

4.2.3 Comparison of winds measured by Doppler lidar and sonic anemometers at SMEAR III and SMEAR IV

Comparisons were made of single range-gate radial Doppler velocity to co-directed sonic anemometer observations at SMEAR III in Helsinki. A profile of 2-D-sonic anemometers (at 31, 35, 43, 59 m a.s.l.) was measuring at the SMEAR III station, ca. 60 m from the Doppler lidar on the roof of FMI (44.4 m a.s.l.). Lidar data from three near-horizontal beam directions (91, 179, 196°) were analysed. The horizontal difference between the centre of the first available lidar range-gate (105 m) of the three beams and the anemometers was 110, 40 and 50 m, respectively. An average value of the two highest anemometers best represents the chosen lidar range-gate which remains < 5 m lower (lidar beam elevation was ≤ 1°). Due to spatial differences of the related velocities we compare 30 min mean winds. Measurements took place from 14

AMTD
6, 7251–7313, 2013

October 2011 to 20 June 2012. The Doppler velocity against the velocity measured with sonic technique show good comparability (Fig. 9, $r > 0.96$), which gives confidence in these Doppler lidar wind measurements. The beam directions with a shorter horizontal separation to the anemometers have a better correspondence with the lidar. Perhaps surprisingly, the anemometer gives slightly lower wind values on average despite a slightly higher height. Overall, these observations are in accordance with similar lidar–sonic comparison measurements performed with a Streamline Doppler lidar in London (Lane et al., 2013; Wood et al., 2013a).

Comparisons were made of single range-gate (7th, i.e. 225 m above the lidar) wind speeds and directions derived from DBS data with values measured with sonic anemometer at the Puijo tower at 220 m height above lake level during 20 September 2011–20 September 2012 (Table 6, Fig. S2, Supplement). Wind speed and direction measured by the two sensors were averaged over half an hour. Linear curve was fitted when wind speed measured by the anemometer was plotted as a function of wind speed derived from Doppler lidar observations (Fig. S2, Supplement). Based on the analysis, the anemometer measured typically higher wind speed values than the Doppler lidar derived values, in contrast to the anemometer at SMEAR III (where for the closest comparison, the lidar slightly over-estimated Doppler velocity). We believe that this consistent small bias may easily be influenced by the spatial difference (2 km) of measurement sites, since more closer correspondence have been observed previously (Angelou et al., 2011). The large bias in wind direction observations was perhaps hence due to non-optimal positioning of the Doppler lidar. Nevertheless, we have accounted for the directional bias in the further analysis. These observations show clearly that the Doppler lidar should be closer to the sonic anemometer to remove the effect of spatial difference in comparison. In future, sites at Vehmasmäki, Hyytiälä and Sodankylä offer the possibility for further nearby comparison with sonic anemometers mounted in towers. It seemed that in the presence of precipitation, correlation between anemometer and lidar measured wind speed decreases (Table 6), which could be due to increased uncertainty in Doppler lidar wind retrievals from falling targets in DBS volume.

AMTD
6, 7251–7313, 2013

4.3 Towards operational applications with the scanning Doppler lidars

4.3.1 Effect of surface roughness on wind field

An advantage of the network is that at all our stations have a clear line-of-site of at least 90°, down close to the horizon. Vertical azimuth display (VAD) and range height indicator (RHI) techniques are used, along with different combinations of custom designed azimuth, elevation and temporal settings. In general our long-term aim is to develop new operational scanning strategies – and subsequent data-analysis methods – to be used with characterisation of ABL phenomena and meteorology, air quality monitoring, cloud physics and weather forecasting. It is clear that other research disciplines such as wave or ice researchers would also benefit from information on temporal and spatial variation of surface wind field.

As an example we have measured a VAD scan every 30 min with elevation of 4°, azimuth differences of 15° and 5 s temporal (i.e. one ray/point) resolution at Utö. Near horizontal scanning over the surface gives us primarily the Doppler velocity field (Fig. 10). With the help of trigonometry we are able to estimate spatially resolved wind speed (U) and direction (φ) fields at each range gate based on radial Doppler velocity measurements (Wood et al., 2013a),

$$v_a = U \cdot \cos(\varphi - \theta_a) \quad (1)$$

$$v_b = U \cdot \cos(\varphi - \theta_b) \quad (2)$$

where v_a and v_b are Doppler velocity vectors of a pair of rays (a and b, respectively). The U is wind speed and φ is the wind direction, which have to be assumed constant between the pair of rays; θ_a and θ_b are ray azimuths from due north.

Due to the 4° beam elevation from lidar horizon, the range-gate height from sea level increases with the increasing distance from the lidar. As an example, at 1.5 km distance the range gate height from lidar horizon is 104 m. When comparing corresponding range gates, and thus altitudes, we see from Fig. 10 how the wind speed and direction

AMTD
6, 7251–7313, 2013

change perhaps due to changing surface from sea to land, and how wind field changes when drifting over sea before and after an island surrounded smaller islands on north and east sides (not shown in the Fig. 10). In future, analysis of long-term statistics of wind evolution over various surfaces enables us characterise the effect of these surfaces on air flow dynamics.

A simple confidence test for the method is to calculate the radial Doppler velocity using Eqs. (1) and (2). Only values of absolute velocity may be calculated because information on sign (i.e. direction) is lost when calculating wind speed and direction (Fig. 10). When investigating differences between calculated and absolute values of measured radial velocity, it is clear that in the directions where wind speed and direction can be calculated from the main component of the velocity vector, we obtain best agreement (Fig. 10). Results in directions of a minor velocity component can be used as indicative only. Nevertheless, these results indicate applicability of the method.

4.3.2 Air-quality monitoring with the Doppler lidars

In spring 2012, three Doppler lidars went operational (Table 1). On 22 May, two Doppler lidars monitored some increased depolarisation ratio values in the non-cloudy ABL, which is indicative of large fraction of non-spherical particles (e.g. fresh road dust or hydrophobic particles). Depolarisation ratio profiles measured in Helsinki showed increased values throughout the ABL, while in Utö a new air mass with highly non-spherical particles appeared into the ABL around 11:00 UTC (Fig. 11). However, at Utö the increased values were observed by in-situ aerosol particle monitors for a short time only after 16:00 UTC. In Kuopio Doppler lidar showed moderate signal from moist ABL aerosol particles only in the co-channel.

Both ground-based and satellite-based AOD (from MODIS_Terra and AQUA at 550 nm) observations showed increased values over the southern Finland. In the middle and northern Finland, the AOD values were close to the long term averages. Further analysis of the aerosol particle dispersion in the ABL (i.e. Doppler lidar backscatter and depolarisation profiles), Doppler lidar vertical air motion, wind speed and direc-

AMTD
6, 7251–7313, 2013

tion profiles, and air mass back-trajectories from the Air Resources Laboratory at the National Oceanic and Atmospheric Administration's Hybrid Single-Particle Lagrangian Integrated Trajectory (HYSPLIT, version 4.8) model (Draxler and Hess, 2004; Air Resources Laboratory, 2011) indicated that, in southern continental Finland, increased depolarisation values could be due to mixture of road dust, which is a typical problem in spring time, and ash transported from forest fires nearby Finnish south-eastern border. However, a dust or ash episode from local sources in Utö is unlikely to cause observed aerosol particle depolarisation ratio profiles. In addition to that, ground-based data were indicative of a change in aerosol particle population due to changing air mass, which was detected by Doppler lidar wind direction profile observations, and appearance of a new mode of 50–150 nm particles. Back-trajectory analysis confirmed that air masses drifted via southern Finland and forest fire areas in western Russia.

This example has demonstrated the capability of the Doppler lidar network for air-quality monitoring purposes. However, the lidar depolarisation ratio method is limited to non- or nearly non-spherical targets, and thus, pollution of hydrophilic particles or particles suspended long enough in the moist ABL are not detected in cross-channel. This may be improved by developing data-analysis methods to deploy raw data instead of measurement software pre-processed data, which is currently used in our data analysis.

5 Concluding remarks

A new ground-based remote sensing network has been established in Finland. The main objectives of the Finland's remote-sensing network are to provide information on aerosol particles, wind, ABL evolution, clouds, precipitation and related processes for now-casting, air quality, public and the aviation-safety authority, and climate prediction. Different to other similar nationwide infrastructures, Finland's remote-sensing network allows research in a variety of environments: (1) from urban to rural to marine environments, and (2) from continental to arctic climates. Instrumentation consists of passive

AMTD
6, 7251–7313, 2013

(e.g. sunphotometers, microwave radiometers) and active (e.g. Doppler lidars, cloud radar, Raman lidar, ceilometers) remote sensors. In addition, extensive possibilities for synergy of in-situ and remote-sensing sensors, and co-operation across research disciplines are advantages to the Finnish remote-sensing infrastructure.

Performance of the Doppler lidars was investigated during two inter-comparison campaigns in Helsinki. Our scope was to investigate comparability of backscatter coefficient and wind quantities, which is important since these instruments are already placed at different sites across Finland. The results indicated good comparability of investigated wind quantities between instruments, and reference in-situ wind observations. However, the backscatter coefficient profiles showed differences between the lidars due to different sensitivity or inaccurate telescope focus. When knowing these differences we are able to consider them in data analysis and subsequent conclusions. In addition, Doppler lidar operational reliability and capability was investigated. Harsh winters and low ambient aerosol particle load limits data coverage. Thus, care must be taken on maintenance during winter and novel data analysis methods are required to be developed.

In future, we expect to continuously extending our ground-based remote sensing-network and improving its capability by developing data processing methods. One of our plans is to increase backscattering profile collection from existing ceilometer network. In the year 2014 a project "Biogenic Aerosols: Effects on Clouds and Climate (BEACC)" will begin in Hyytälä. The project hosts comprehensive ground-based remote-sensing facility ARM Climate Research Facility. Meanwhile, full capability of the current instrumentation will be deployed.

Supplementary material related to this article is available online at http://www.atmos-meas-tech-discuss.net/6/7251/2013/amtd-6-7251-2013-supplement.pdf.

AMTD
6, 7251–7313, 2013

Acknowledgements. The research leading to these results has received funding from the European Union Seventh Framework Programme (FP7/2007–2013) under grant agreement no. 262254 (ACTRIS), the Academy of Finland, Center of Excellence Program (project 1118615) and the Academy of Finland FIRI-funding "Infrastructure of Environmental and Atmospheric Sciences" (ATM-Science, project 141451). Curtis Wood acknowledges funding from EC FP7 ERC Grant 227915 (Atmospheric planetary boundary layers – physics, modelling and role in 6 Earth system). People maintaining the SMEAR, Utö and Sodankylä stations are acknowledged.

The service charges for this open access publication have been covered by a Research Centre of the Helmholtz Association.

References

Aaltonen, V., Rodriguez, E., Kazadzis, S., Arola, A., Amiridis, V., Lihavainen, H., and de Leeuw, G.: On the variation of aerosol properties over Finland based on the optical columnar measurements, Atmos. Res., 116, 46–55, doi:10.1016/j.atmosres.2011.07.014, 2012.

Aarnio, P., Yli-Tuomi, T., Kousa, A., Mäkelä, T., Hirsikko, A., Hämeri, K., Räisänen, M., Hillamo, R., Koskentalo, T., and Jantunen, M.: The concentrations and composition of and exposure to fine particles ($PM_{2.5}$) in the Helsinki subway system, Atmos. Environ., 39, 5059–5066, 2005.

ACIA: Arctic Climate Impact Assessment, Cambridge University Press, New York, USA, 2005.

Air Resources Laboratory: Gridded Meteorological Data Archives, available at: http://www.arl.noaa.gov/archives.php (last access: 31 August 2012), 2011.

Albrecht, B. A.: Aerosols, cloud microphysics, and fractional cloudiness, Science, 245, 1227–1230, 1989.

Althausen, D., Engelmann, R., Baars, H., Heese, B., Ansmann, A., Müller, D., and Komppula, M.: Portable Raman Lidar Polly^{XT} for Automated Profiling of Aerosol Backscatter, Extinction, and Depolarization, J. Atmos. Ocean. Tech., 26, 2366–2378, doi:10.1175/2009JTECHA1304.1, 2009.

Angelou, N., Bingöl, F., Courtney, M., Diznabi, B., Foussekis, D., Gottschall, D., Hansen, K. H., Jørgensen, H. E., Kristensen, L., Larsen, G. C., Lindelöw-Marsden, P., Mann, J.,

AMTD
6, 7251–7313, 2013

Mikkelsen, T., Paulsen, U. S., Pedersen, T. F., Peña, A., Sathe, A., Sjöholm, M., and Wagner, R.: Advancements in wind energy metrology UPWIND 1A2.3, in: Risø-R-1752(EN), edited by: Pedersen, T. F. and Wagner, R., Technical University Denmark, Risø National laboratory for Sustainable Energy, Risø, Denmark, 2011.

Ansmann, A., Tesche, M., Seifer, P., Gross, S., Freudenthaler, V., Apituley, A., Wilson, K. M., Serikov, I., Linné, H., Heinold, B., Hiebsch, A., Schnell, F., Schmidt, J., Mattis, I., Wandinger, U., and Wiegner, M.: Ash and fine-mode particle mass profiles from EARLINET-AERONET observations over central Europe after the eruptions of the Eyjafjallajökull volcano in 2010, J. Geophys. Res., 116, D00U02, doi:10.1029/2010JD015567, 2011.

Banta, R. M., Pichugina, Y. L., and Brewer, W. A.: Turbulent velocity-variance profiles in the stable boundary layer generated by a nocturnal low-level jet, J. Atmos. Sci., 63, 2700–2719, 2006.

Barlow, J. F., Dunbar, T. M., Nemitz, E. G., Wood, C. R., Gallagher, M. W., Davies, F., O'Connor, E., and Harrison, R. M.: Boundary layer dynamics over London, UK, as observed using Doppler lidar during REPARTEE-II, Atmos. Chem. Phys., 11, 2111–2125, doi:10.5194/acp-11-2111-2011, 2011.

Barlow, J. and Coceal, O.: A review of urban roughness sublayer turbulence, Met Office Tech. Rep., Exeter, 68 pp., 2009.

Bony, S., Colman, R., Kattsov, V. M., Allan, R. P., Bretherton, C. S., Dufresne, J.-L., Hall, A., Hallegatte, S., Holland, M. M., Ingram, W., Randall, D. A., Soden, B. J., Tselioudis, G., and Webb, M. J.: How well do we understand and evaluate climate change feedback processes?, J. Climate, 19, 3445–3482, 2006.

Chen, Y. and Penner, J. E.: Uncertainty analysis for estimates of the first indirect aerosol effect, Atmos. Chem. Phys., 5, 2935–2948, doi:10.5194/acp-5-2935-2005, 2005.

Chiu, J. C., Huang, H.-C., Marshak, A., Slutsker, I., Giles, D. M., Holben, B. N., Knyazikhin, Y., and Wiscombe, W. J.: Cloud optical depth retrievals from the Aerosol Robotic Network (AERONET), J. Geophys. Res., 115, D14202, doi:10.1029/2009JD013121, 2010.

Collier, C. G., Davies, F., and Pearson, G. N.: The land below the wind: Doppler LIDAR observations from the tropical rain forest of Sabah, Borneo, Malaysia, R. Met. S. Weather, 65, 45–50, 2010.

Dal Maso, M., Hyvärinen, A., Komppula, M., Tunved, P., Kerminen, V.-M., Lihavainen, H., Viisanen, Y., Hansson, H.-C., and Kulmala, M.: Annual and interannual variation in boreal forest

AMTD
6, 7251–7313, 2013

aerosol particle number and volume concentration and their connection to particle formation, Tellus B, 60, 495–508, 2008.
Delanoë, J., Hogan, R. J., Forbes, R. M., Bodas-Salcedo, A., and Stein, T. H. M.: Evaluation of ice cloud representation in the ECMWF and UK Met Office models using CloudSat and CALIPSO data, Q. J. Roy. Meteorol. Soc., 137, 2064–2078, 2011.
Devenish, B. J., Thomson, D. J., Marenco, F., Leadbetter, S. J., Ricketts, H., and Dacre, H. F.: A study of the arrival over the UK in April 2010 of the Eyjafjallakull ash cloud using ground-based lidar and numerical simulation, Atmos. Environ., 48, 152–164, 2012.
Draxler, R. R. and Hess, G. D.: Description of the HYSPLIT 4 Modelling System, NOAA Technical Memorandum ERL ARL–224, Air Resources Laboratory, Silver Spring, Maryland, 2004.
Engelmann, R., Althausen, D., Heese, B., Baars, H., and Komppula, M.: Recent upgrades of the multiwavelength polarization Raman lidar Polly^{XT}, in: Proceedings of the International Laser Radar Conference, Porto Heli, Greece, 2012.
Engler, C., Lihavainen, H., Komppula, M., Kerminen, V.-M., and Kulmala, M.: Continuous measurements of aerosol properties at the Baltic Sea, Tellus B, 59, 728–741, 2007.
Flentje, H., Heese, B., Reichardt, J., and Thomas, W.: Aerosol profiling using the ceilometer network of the German Meteorological Service, Atmos. Meas. Tech. Discuss., 3, 3643–3673, doi:10.5194/amtd-3-3643-2010, 2010.
Ghamberg, M., Savijärvi, H., and Leskinen, M.: The influence of synoptic scale flow on sea breeze induced surface winds and calm zones, Tellus A, 62, 209–217, 2010.
Görsdorf, U., Lehmann, V., Bauer-Pfundstein, M., and Peters, G.: A 35 GHz radar for long term observations of cloud parameters – Description of system, data processing and sampling strategy, Am. Meteorol. Soc., in preparation, 2013.
Hari, P. and Kulmala, M.: Station for Measuring Ecosystem–Atmosphere Relations (SMEAR II), Boreal Environ. Res., 10, 315–322, 2005.
Hegg, D. A., Covert, D. S., Jonsson, H. H., and Woods, R. K.: A simple relationship between cloud drop number concentration and precursor aerosol concentration for the regions of Earth's large marine stratocumulus decks, Atmos. Chem. Phys., 12, 1229–1238, doi:10.5194/acp-12-1229-2012, 2012.
Heymsfield, A. J., Bansemer, A., Field, P. R., Durden, S. L., Stith, J. L., Dye, J. E., Hall, W., and Grainger, C. A.: Observations and parametrizations of particle size distributions in deep tropical cirrus and stratiform precipitating clouds: results from in situ observations in TRMM field campaigns, J. Atmos. Sci., 59, 3457–3491, 2002.

AMTD
6, 7251–7313, 2013

Heywood, J. and Boucher, O.: Estimates of the direct and indirect radiative forcing due to tropospheric aerosols: a review, Rev. Geophys., 38, 513–543, 2000.
Hirsikko, A., Vakkari, V., Tiitta, P., Hatakka, J., Kerminen, V.-M., Sundström, A.-M., Beukes, J. P., Manninen, H. E., Kulmala, M., and Laakso, L.: Multiple daytime nucleation events in semi-clean savannah and industrial environments in South Africa: analysis based on observations, Atmos. Chem. Phys., 13, 5523–5532, doi:10.5194/acp-13-5523-2013, 2013.
Hogan, R. J., Grant, A. L. M., Illingworth, A. J., Pearson, G. N., and O'Connor, E. J.: Vertical velocity variance and skewness in clear and cloud-topped boundary layers as revealed by Doppler lidar, Q. J. Roy. Meteorol. Soc., 135, 635–643, 2009.
Holben, B. N., Eck, T. F., Slutsker, I., Tanré, D., Buisk, J. P., Setzer, A., Vermote, E., Reagan, J. A., Kaufman, Y. J., Nakajima, T., Lavenu, F., Jankowiak, I., and Smirnov, A.: AERONET – a federated instrument network and data archive for aerosol characterization, Remote Sens. Environ., 66, 1–16, 1998.
Hou, A. Y., Skofronick-Jackson, G., Kummerow, C. D., and Shepherd, J. M.: Global precipitation measurements, in: Precipitation: Advances in Measurement, Estimation and Prediction, edited by: Michaelides, S., Springer-Verlag, Berlin, Heidelberg, 2008.
Hussein, T., Kukkonen, J., Korhonen, H., Pohjola, M., Pirjola, L., Wraith, D., Härkönen, J., Teinilä, K., Koponen, I. K., Karppinen, A., Hillamo, R., and Kulmala, M.: Evaluation and modeling of the size fractionated aerosol particle number concentration measurements nearby a major road in Helsinki – Part II: Aerosol measurements within the SAPPHIRE project, Atmos. Chem. Phys., 7, 4081–4094, doi:10.5194/acp-7-4081-2007, 2007.
Hyvärinen, A.-P., Komppula, M., Engler, C., Kivekäs, N., Kerminen, V.-M., Dal Maso, M., Viisanen, Y., and Lihavainen, H.: Atmospheric new particle formation at Utö, Baltic Sea 2003–2005, Tellus B, 60, 345–352, 2008.
Illingworth, A. J., Hogan, R. J., O'Connor, E. J., Bouniol, D., Brooks, M. E., Delanoë, J., Donovan, D. P., Eastment, J. D., Gaussiat, N., Goddard, J. W. F., Haeffelin, M., Klein baltink, H., Krasnov, O. A., Pelon, J., Piriou, J.-M., Protat, A., Russchenberg, H. W. J., Seifert, A., Tompkins, A. M., van Zadelhoff, G.-J., Vinit, F., Willén, U., Wilson, D. R., and Wrench, C. L.: CLOUDNET: continuous evaluation of cloud profiles in seven operational models using ground-based observations, B. Am. Meteorol. Soc., 88, 883–898, doi:10.1175/BAMS-88-6-883, 2007.

AMTD
6, 7251–7313, 2013

Ilvesniemi, H., Levula, J., Ojansuu, R., Kolari, P., Kulmala, L., Pumpanen, J., Launiainen, S., Vesala, T., and Nikinmaa, E.: Long-term measurements of the carbon balance of a boreal Scots pine dominated forest ecosystem, Boreal Environ. Res., 14, 731–753, 2009.
Ilvesniemi, H., Pumpanen, J., Duursma, R., Hari, P., Keronen, P., Kolari, P., Kulmala, M., Mammarella, I., Nikinmaa, E., Rannik, Ü., Pohja, T., Siivola, E., and Vesala, T.: Water balance of a boreal Scots pine forest, Boreal Environ. Res., 15, 375–396, 2010.
Immler, F., Treffeisen, R., Engelbart, D., Krüger, K., and Schrems, O.: Cirrus, contrails, and ice supersaturated regions in high pressure systems at northern mid latitudes, Atmos. Chem. Phys., 8, 1689–1699, doi:10.5194/acp-8-1689-2008, 2008.
IPCC: Solomon, S., Qin, D., Manning, M., Chen, Z., Marquis, M., Averyt, K. B., Tignor, M., and Miller, H. L. (Eds.): Climate Change 2007: The Physical Science Basis, Contribution of Working Group I to the Fourth Assessment Report of the Intergovernmental Panel on Climate Change, Cambridge University Press, Cambridge, UK and New York, NY, USA, 996 pp., 2007.
Janssen, R. H. H., Vil Janssen, R. H. H., Vila-Guerau de Arellano, J., Ganzeveld, L. N., Kabat, P., Jimenez, J. L., Farmer, D. K., van Heerwaarden, C. C., and Mammarella, I.: Combined effects of surface conditions, boundary layer dynamics and chemistry on diurnal SOA evolution, Atmos. Chem. Phys., 12, 6827–6843, doi:10.5194/acp-12-6827-2012, 2012.
Järvi, L., Rannik, Ü., Mammarella, I., Sogachev, A., Aalto, P. P., Keronen, P., Siivola, E., Kulmala, M., and Vesala, T.: Annual particle flux observations over a heterogeneous urban area, Atmos. Chem. Phys., 9, 7847–7856, doi:10.5194/acp-9-7847-2009, 2009a.
Järvi, L., Hannuniemi, H., Hussein, T., Junninen, H., Aalto, P. P., Hillamo, R., Mäkelä, T., Keronen, P., Siivola, E., Vesala, T., and Kulmala, M.: The urban measurement station SMEAR III: continuous monitoring of air pollution and surface–atmosphere interactions in Helsinki, Finland, Boreal Environ. Res., suppl. A, 14, 86–109, 2009b.
Järvi, L., Nordbo, A., Junninen, H., Riikonen, A., Moilanen, J., Nikinmaa, E., and Vesala, T.: Seasonal and annual variation of carbon dioxide surface fluxes in Helsinki, Finland, in 2006–2010, Atmos. Chem. Phys., 12, 8475–8489, doi:10.5194/acp-12-8475-2012, 2012.
Juga, I., Hippi, M., Moisseev, D., and Saltikoff, E.: Analysis of weather factors responsible for the traffic "Black Day" in Helsinki, Finalnd, on 17 March 2005, Meteorol. Appl., 19, 1–9, 2012.
Kamphus, M., Ettner-Mahl, M., Klimach, T., Drewnick, F., Keller, L., Cziczo, D. J., Mertes, S., Borrmann, S., and Curtius, J.: Chemical composition of ambient aerosol, ice residues and cloud droplet residues in mixed-phase clouds: single particle analysis during the Cloud

AMTD
6, 7251–7313, 2013

and Aerosol Characterization Experiment (CLACE 6), Atmos. Chem. Phys., 10, 8077–8095, doi:10.5194/acp-10-8077-2010, 2010.
Kivi, R., Kyrö, E., Turunen, T., Ulich, T., and Turunen, E.: Atmospheric trends above Finland: II troposphere and stratosphere, Geophysica, 35, 71–85, 1999.
Kolmonen, P., Sundström, A.-M., Sogacheva, L., Rodriguez, E., Virtanen, T., and de Leeuw, G.: Uncertainty characterization of AOD for the AATSR dual and single view retrieval algorithms, Atmos. Meas. Tech. Discuss., 6, 4039–4075, doi:10.5194/amtd-6-4039-2013, 2013.
Komppula, M., Mielonen, T., Arola, A., Korhonen, K., Lihavainen, H., Hyvärinen, A.-P., Baars, H., Engelmann, R., Althausen, D., Ansmann, A., Müller, D., Panwar, T. S., Hooda, R. K., Sharma, V. P., Kerminen, V.-M., Lehtinen, K. E. J., and Viisanen, Y.: Technical Note: One year of Raman-lidar measurements in Gual Pahari EUCAARI site close to New Delhi in India – Seasonal characteristics of the aerosol vertical structure, Atmos. Chem. Phys., 12, 4513–4524, doi:10.5194/acp-12-4513-2012, 2012.
Korhonen, K., Giannakaki, E., Mielonen, T., Pfüller, A., Laakso, L., Vakkari, V., Baars, H., Engelmann, R., Beukes, J. P., Van Zyl, P. G., Ramandh, A., Ntsangwane, L., Josipovic, M., Tiitta, P., Fourie, G., Ngwana, I., Chiloane, K., and Komppula, M.: Atmospheric boundary layer top height in South Africa: measurements with lidar and radiosonde compared to three atmospheric models, Atmos. Chem. Phys. Discuss., 13, 17407–17450, doi:10.5194/acpd-13-17407-2013, 2013.
Koskinen, J. T., Poutiainen, J., Schultz, D. M., Joffre, S., Koistinen, J., Saltikoff, E., Gregow, E., Turtiainen, H., Dabberdt, W. F., Damski, J., Eresmaa, N., Göke, S., Hyvärinen, O., Järvi, L., Karppinen, A., Kotro, J., Kuitunen, T., Kukkonen, J., Kulmala, M., Moisseev, D., Nurmi, P., Pohjola, H., Pylkkö, P., Vesala, T., and Viisanen, Y.: The Helsinki TESTBED, B. Am. Meteorol. Soc., 92, 325–342, doi:10.1175/2010BAMS2878.1, 2011.
Kulmala, M. and Tammet, H.: Finnish–Estonian air ion and aerosol workshops, Boreal Environ. Res., 12, 237–245, 2007.
Kulmala, M., Hämeri, K., Aalto, P. P., Mäkelä, J. M., Pirjola, L., Nilsson, E. D., Buzorius, G., Rannik, Ü., Dal Maso, M., Seidl, W., Hoffman, T., Janson, R., Hansson, H.-C., Viisanen, Y., Laaksonen, A., and O'Dowd, C. D.: Overview of the international project on biogenic aerosol formation in the boreal forest (BIOFOR), Tellus B, 53, 324–343, 2001.
Laitinen, T., Ehn, M., Junninen, H., Ruiz-Jimenez, J., Prshintsev, J., Hartonen, K., Riekkola, M.-L., Worsnop, D. R., and Kulmala, M.: Characterization of organic compounds in 10- to 50-nm

AMTD
6, 7251–7313, 2013

aerosol particles in boreal forest with laser desorption-ionization aerosol mass spectrometer and comparison with other techniques, Atmos. Environ., 45, 3711–3719, 2011.
Lane, S. E., Barlow, J. F., and Wood, C. R.: An assessment of a three-beam Doppler lidar wind profiling method for use in urban areas, J. Wind Eng. Ind. Aerod., 119, 53–59, 2013.
Launiainen, S.: Seasonal and inter-annual variability of energy exchange above a boreal Scots pine forest, Biogeosciences, 7, 3921–3940, doi:10.5194/bg-7-3921-2010, 2010.
Leskinen, A., Portin, H., Komppula, M., Miettinen, P., Arola, A., Lihavainen, H., Hatakka, J., Laaksonen, A., and Lehtinen, K. E. J.: Overview of the research activities and results at Puijo semi-urban measurement station, Boreal Environ. Res., 14, 576–590, 2009.
Leskinen, A., Arola, A., Komppula, M., Portin, H., Tiitta, P., Miettinen, P., Romakkaniemi, S., Laaksonen, A., and Lehtinen, K. E. J.: Seasonal cycle and source analyses of aerosol optical properties in a semi-urban environment at Puijo station in Eastern Finland, Atmos. Chem. Phys., 12, 5647–5659, doi:10.5194/acp-12-5647-2012, 2012.
Leskinen, M., Markkula, I., Koistinen, J., Pylkkö, P., Ooperi, S., Siljamo, P., Ojanen, H., Raiskio, S., and Tiilikkala, K.: Pest insect immigration warning by an atmospheric dispersion model, weather radars and traps, J. Appl. Entoml., 135, 55–67, 2011.
Lihavainen, H., Kerminen, V.-M., and Remer, L. A.: Aerosol-cloud interaction determined by both in situ and satellite data over a northern high-latitude site, Atmos. Chem., 10, 10987–10995, 2010.
Lohmann, U. and Feichter, J.: Global indirect aerosol effects: a review, Atmos. Chem. Phys., 5, 715–737, doi:10.5194/acp-5-715-2005, 2005.
Lohmann, U., Rotstayn, L., Storelvmo, T., Jones, A., Menon, S., Quaas, J., Ekman, A. M. L., Koch, D., and Ruedy, R.: Total aerosol effect: radiative forcing or radiative flux perturbation?, Atmos. Chem. Phys., 10, 3235–3246, doi:10.5194/acp-10-3235-2010, 2010.
Madonna, F., Amodeo, A., Boselli, A., Cornacchia, C., Cuomo, V., D'Amico, G., Giunta, A., Mona, L., and Pappalardo, G.: CIAO: the CNR-IMAA advanced observatory for atmospheric research, Atmos. Meas. Tech., 4, 1191–1208, doi:10.5194/amt-4-1191-2011, 2011.
Makkonen, R., Asmi, A., Kerminen, V.-M., Boy, M., Arneth, A., Hari, P., and Kulmala, M.: Air pollution control and decreasing new particle formation lead to strong climate warming, Atmos. Chem. Phys., 12, 1515–1524, doi:10.5194/acp-12-1515-2012, 2012.
Manninen, H. E., Petäjä, T., Asmi, E., Riipinen, I., Nieminen, T., Mikkilä, J., Hõrrak, U., Mirme, A., Mirme, S., Laakso, L., Kerminen, V.-M., and Kulmala, V.-M.: Long-term field measurements

AMTD
6, 7251–7313, 2013

of charged and neutral clousters using Neutral cluster and Air Ion Spectrometer (NAIS), Boreal Environ. Res., 14, 591–605, 2009.
Marinoni, A., Laj, P., Sellegri, K., and Mailhot, G.: Cloud chemistry at the Puy de Dôme: variability and relationships with environmental factors, Atmos. Chem. Phys., 4, 715–728, doi:10.5194/acp-4-715-2004, 2004.
McFiggans, G., Artaxo, P., Baltensperger, U., Coe, H., Facchini, M. C., Feingold, G., Fuzzi, S., Gysel, M., Laaksonen, A., Lohmann, U., Mentel, T. F., Murphy, D. M., O'Dowd, C. D., Snider, J. R., and Weingartner, E.: The effect of physical and chemical aerosol properties on warm cloud droplet activation, Atmos. Chem. Phys., 6, 2593–2649, doi:10.5194/acp-6-2593-2006, 2006.
McLaughlin, D. J., Knapp, E. A., Wang, Y., and Chandrasekar, V.: Distributed weather radar using X-band active arrays, IEEE Aero. El. Sys. Mag., 7, 21–26, 2009.
Milroy, C., Martucci, G., Lolli, S., Loaec, S., Sauvage, L., Xueref-Remy, I., Lavrič, J. V., Ciais, P., and O'Dowd, C. D.: On the ability of pseudo-operational ground-based light detection and ranging (LIDAR) sensors to determine boundary-layer structure: intercomparison and comparison with in-situ radiosounding, Atmos. Meas. Tech. Discuss., 4, 563–597, doi:10.5194/amtd-4-563-2011, 2011.
Müller, D, Wandinger, U., and Ansmann, A.: Microphysical particle parameters from extinction and backscatter lidar data by inversion with regularization: theory, Appl. Optics, 38, 2346–2357, 1999.
Müller, D., Wandinger, U., Althausen, D., and Fiebig, M.: Comprehensive particle characterization from three-wavelength Raman-lidar observations: case study, Appl. Optics, 40, 4863–4869, 2001.
Myhre, G.: Consistency between satellite-derived and modelled estimates of the direct aerosol effect, Science, 325, 187–190, doi:10.1126/science.1174461, 2009.
Newsom, R. K.: Doppler Lidar (DL) Handbook, DOE/SC-ARM-TR-101, ARM Climate Research Facility, USA, 2012.
Nordbo, A., Järvi, L., and Vesala, T.: Revised eddy covariance flux methodologies – effect on urban energy balance, Tellus B, 64, 18184, doi:10.3402/tellusb.v64i0.18184, 2012.
O'Connor, E. J., Illingworth, A. J., and Hogan, R. J.: A technique for autocalibration of cloud lidar, J. Atmos. Ocean. Tech., 21, 777–786, 2004.
O'Connor, E. J., Hogan, R. J., and Illingworth, A. J.: Retrieving stratocumulus drizzle parameters using Doppler radar and lidar, J. Appl. Meteorol., 44, 14–27, 2005.

AMTD
6, 7251–7313, 2013

O'Connor, E. J., Illingworth, A. J., Brooks, I. M., Westbrook, C. D., Hogan, R. J., Davies, F., and Brooks, B. J.: A method for estimating the turbulent kinetic energy dissipation rate from a vertically pointing Doppler lidar, and independent evaluation from balloon-borne in situ measurements, J. Atmos. Ocean. Tech., 27, 1652–1664, 2010.

Pappalardo, G., Mona, L., D'Amico, G., Wandinger, U., Adam, M., Amodeo, A., Ansmann, A., Apituley, A., Alados Arboledas, L., Balis, D., Boselli, A., Bravo-Aranda, J. A., Chaikovsky, A., Comeron, A., Cuesta, J., De Tomasi, F., Freudenthaler, V., Gausa, M., Giannakaki, E., Giehl, H., Giunta, A., Grigorov, I., Groß, S., Haeffelin, M., Hiebsch, A., Iarlori, M., Lange, D., Linné, H., Madonna, F., Mattis, I., Mamouri, R.-E., McAuliffe, M. A. P., Mitev, V., Molero, F., Navas-Guzman, F., Nicolae, D., Papayannis, A., Perrone, M. R., Pietras, C., Pietruczuk, A., Pisani, G., Preißler, J., Pujadas, M., Rizi, V., Ruth, A. A., Schmidt, J., Schnell, F., Seifert, P., Serikov, I., Sicard, M., Simeonov, V., Spinelli, N., Stebel, K., Tesche, M., Trickl, T., Wang, X., Wagner, F., Wiegner, M., and Wilson, K. M.: Four-dimensional distribution of the 2010 Eyjafjallajökull volcanic cloud over Europe observed by EARLINET, Atmos. Chem. Phys., 13, 4429–4450, doi:10.5194/acp-13-4429-2013, 2013.

Pearson, G., Davies, F., and Collier, C.: An analysis of the performance of the UFAM pulsed Doppler lidar for observing the boundary layer, J. Atmos. Ocean. Tech., 26, 240–250, 2009.

Petäjä, T., Laakso, L., Grönholm, T., Launiainen, S., Evele-Peltoniemi, I., Virkkula, A., Leskinen, A., Backman, J., Manninen, H. E., Sipilä, M., Haapanala, S., Hämeri, K., Vanhala, E., Tuomi, T., Paatero, J., Aurela, M., Hakola, H., Makkonen, U., Hellén, H., Hillamo, R., Vira, J., Prank, M., Sofiev, M., Siitari-Kauppi, M., Laaksonen, A., Lehtinen, K. E. J., Kulmala, M., Viisanen, Y., and Kerminen, V.-M.: In-situ observations of Eyjafjallakull ash paticles by hot-air balloon, Atmos. Environ., 48, 104–112, 2012.

Portin, H. J., Komppula, M., Leskinen, A. P., Romakkaniemi, S., Laaksonen, A., and Lehtinen, K. E. J.: Observations of aerosol-cloud interactions at the Puijo semi-urban measurement station, Boreal Environ. Res., 14, 641–653, 2009.

Remer, L. A., Kaufman, Y. J., Tanré, D., Mattoo, S., Chu, D. A., Martins, J. V., Li, R.-R., Ichoku, C., Levy, R. C., Kleidman, R. G., Eck, T. F., Vermote, E., and Holben, B. N.: The MODIS aerosol algorithm, products, and validation, J. Atmos. Sci., 62, 947–973, 2005.

Revuelta, M. A., Sastre, M., Fernández, A. J., Martín, L., García, R., Gómez-Morena, F. J., Artíñano, B., Pujadas, M., and Molero, F.: Characterization of the Eujafjallakull volcano plume over the Iberian Peninsula by lidar remote sensing and groun-level data collection, Atmos. Environ., 48, 46–55, 2012.

AMTD
6, 7251–7313, 2013

Rolf, C., Krämer, M., Schiller, C., Hildebrandt, M., and Riese, M.: Lidar observation and model simulation of a volcanic-ash-induced cirrus cloud during the Eyjafjallajökull eruption, Atmos. Chem. Phys., 12, 10281–10294, doi:10.5194/acp-12-10281-2012, 2012.

Rose, T. and Czekala, H.: RPG-XCH-DP X frequency, dual polarized radiometer (6.925/10.65/18.70 (21.00)/36.50 GHz h/v), Operating manual, Version 6.8, Radiometer Physics GmbH, Germany, 18 February 2009.

Saltikoff, E. and Nevvonen, L.: First experiences of the operastional use of a dual-polarisation weather radar in Finland, Meteorol. Z., 20, 323–333, 2011.

Saltikoff, E., Tuovinen, J.-P., Kotro, J., Kuitunen, T., and Hohti, H.: A climatological comparison of radar and ground observations of hails in Finland, J. Appl. Meteorol. Clim., 49, 101–114, 2010.

Schobesberger, S., Väänänen, R., Leino, K., Virkkula, A., Backman, J., Pohja, J., Siivola, E., Franchin, A., Mikkilä, J., Paramonov, M., Aalto, P. P., Krejci, R., Petäjä., T., and Kulmala, M.: Airborne measurements over the boreal forest of southern Finland during new particle formation events in 2009 and 2010, Boreal Environ. Res., 18, 145–163, 2013.

Shupe, M. D., Turner, D., Walden, V. P., Bennartz, R., Cadeddu, M. P., Castellani, B. B., Cox, C. J., Hudak, D. R., Kulie, M. S., Miller, N. B., Neely III, R. R., Neff, W. D., and Rowe, P. M.: High and dry, new observations of tropospheric and cloud properties above the Greenland ice sheet, B. Am. Meteorol. Soc., 94, 169–186, 2013.

Sicard, M., Guerrero-Rascado, J. L., Navas-Guzmán, F., Preißler, J., Molero, F., Tomás, S., Bravo-Aranda, J. A., Comerón, A., Rocadenbosch, F., Wagner, F., Pujadas, M., and Alados-Arboledas, L.: Monitoring of the Eyjafjallajökull volcanic aerosol plume over the Iberian Peninsula by means of four EARLINET lidar stations, Atmos. Chem. Phys., 12, 3115–3130, doi:10.5194/acp-12-3115-2012, 2012.

Souch, C. and Grimmond, S.: Applied climatology: urban climate, Prog. Phys. Geog., 30, 270–279, 2006.

Stull, R. B.: An Introduction to Boundary Layer Meteorology, Kluwer Academic Publishers, Dordrecht, the Nederlands, 1988.

Sundström, A.-M., Nousiainen, T., and Petäjä, T.: On the quantitative low-level aerosol measurements using a ceilometer-type lidar, Atmos. Ocean. Tech., 26, 2340–2352, doi:10.1175/2009JTECHA1252.1, 2009.

Twomey, S.: Pollution and the planetary albedo, Atmos. Environ., 8, 1251–1256, 1974.

AMTD
6, 7251–7313, 2013

Vaisala: Ceilometer CT25K User's Guide, Vaisala, available at: http://www.rish.kyoto-u.ac.jp/ear/ceilometer/ct25k.pdf, last access: 26 February 1999.

Verheggen, B., Cozic, J., Weingartner, E., Bower, K., Mertes, S., Connolly, P., Gallagher, M., Flynn, M., Choularton, T., and Baltensberger, U.: Aerosol partitioning between the interstitial and the condensed phase in mixed-phase clouds, J. Geophys. Res., 112, D23202, doi:10.1029/2007JD008714, 2007.

Vesala, T., Haataja, J., Aalto, P., Altimir, N., Buzorius, G., Garam, E., Hämeri, K., Ilvesniemi, H., Jokinen, V., Keronen, P., Lahti, T., Markkanen, T., Mäkelä, J. M., Nikinmaa, E., Palmroth, S., Palva, L., Pohja, T., Pumpanen, J., Rannik, U., Siivola, E., Ylitalo, H., Hari, P., and Kulmala, M.: Long-term field measurements of atmosphere-surface interactions in boreal forest combining forest ecology, micrometeorology, aerosol physics and atmospheric chemistry, Trends Heat, Mass Moment Trans., 4, 17–35, 1998.

Weitkamp, C.: Lidar: Range-Resolved Optical Remote Sensing of the Atmosphere, Springer series of Optical Sciences, vol. 102, Springer, 460 pp., 2005.

Westbrook, C. D., Illingworth, A. J., O'Connor, E. J., and Hogan, R. J.: Doppler lidar measurements of oriented planar ice crystals falling from supercooled and glaciated layer clouds, Q. J. Roy. Meteorol. Soc., 136, 260–276, 2010a.

Westbrook, C. D., Illingworth, A. J., O'Connor, E. J., and Hogan, R. J.: Doppler lidar measurements of oriented planar ice crystals falling from supercooled and glaciated layer clouds, Q. J. Roy. Meteorol. Soc., 136, 260–276, 2010b.

Williams, J., Crowley, J., Fischer, H., Harder, H., Martinez, M., Petäjä, T., Rinne, J., Bäck, J., Boy, M., Dal Maso, M., Hakala, J., Kajos, M., Keronen, P., Rantala, P., Aalto, J., Aaltonen, H., Paatero, J., Vesala, T., Hakola, H., Levula, J., Pohja, T., Herrmann, F., Auld, J., Mesarchaki, E., Song, W., Yassaa, N., Nölscher, A., Johnson, A. M., Custer, T., Sinha, V., Thieser, J., Pouvesle, N., Taraborrelli, D., Tang, M. J., Bozem, H., Hosaynali-Beygi, Z., Axinte, R., Oswald, R., Novelli, A., Kubistin, D., Hens, K., Javed, U., Trawny, K., Breitenberger, C., Hidalgo, P. J., Ebben, C. J., Geiger, F. M., Corrigan, A. L., Russell, L. M., Ouwersloot, H. G., Vilà-Guerau de Arellano, J., Ganzeveld, L., Vogel, A., Beck, M., Bayerle, A., Kampf, C. J., Bertelmann, M., Köllner, F., Hoffmann, T., Valverde, J., González, D., Riekkola, M.-L., Kulmala, M., and Lelieveld, J.: The summertime Boreal forest field measurement intensive (HUMPPA-COPEC-2010): an overview of meteorological and chemical influences, Atmos. Chem. Phys., 11, 10599–10618, doi:10.5194/acp-11-10599-2011, 2011.

Wood, C. R.: Adapting our cities for future climates, Weather, 65, 307–309, 2010.

AMTD
6, 7251–7313, 2013

Wood, C. R., Arnold, S. J., Balogun, A. A., Barlow, J. F., Belche, S. E., Britter, R. E., Cheng, H., Dobre, A., Lingard, J. J. N., Martin, D., Neophytou, M., Petersson, F. K., Robins, A. G., Shallcross, D. E., Smalley, R. J., Tate, J. E., Tomlin, A. S., and White, I. R.: Dispersion experiments in central London: the 2007 DAPPLE project, B. Am. Meteorol. Soc., 90, 955–969, 2009a.

Wood, C. R., O'Connor, E. J., Hurley, R., Reynolds, D. R., and Illingworth, A. J.: Cloud-radar observations of insects in the UK convective boundary layer, Meteorol. Appl., 16, 491–500, 2009b.

Wood, C. R., Pauscher, L., Ward, H. C., Kotthaus, S., Barlow, J. F., Gouvea, M., Lane, S. E., and Grimmond, C. S. B.: Wind observations above an urban river using a new lidar technique, scintillometry and anemometry, Sci. Total Environ., 442, 527–533, 2013a.

Wood, C., Järvi, L., Kouznetsov, R., Nordbo, A., Drebs, A., Vihma, T., Hirsikko, A., Suomi, I., Fortelius, C., O'Connor, E., Haapanala, S., Moilanen, J., Kangas, M., Karppinen, A., Joffre, S., Vesala, T., and Kukkonen, J.: An overview on the Urban Boundary-layer Atmosphere Network in Helsinki, B. Am. Meteorol. Soc., doi:10.1175/BAMS-D-12-00146.1, in press, 2013b.

van Ulden, A. P. and Wieringa, J.: Atmospheric boundary layer research at Cabauw, Bound.-Lay. Meteorol., 78, 39–69, 1996.

AMTD
6, 7251–7313, 2013

Table 1. Summary of the measurement sites within Finland's ground-based remote-sensing network: AWS stands for automatic weather station. Doppler lidars are from HALO Photonics. Statistics of the average annual temperature, rain amount and wintertime snow depth are from FMI archive.

Site	Site description	Remote sensing instruments
Helsinki (SMEAR III) – 60.20° N – 24.96° E – 45 m a.s.l.	Urban environment with inhomogeneous topography, marine and continental influenced climate. Annual average temperature is > 5 °C, average wintertime snow depth is 10–20 cm. Annual rain amount is 900–1100 mm.	1. Doppler lidar: since 1 Sep 2011 2. Doppler cloud radar (Mira-35S): test campaign: 8 Sep 2011–31 Mar 2012 3. Ceilometer profiles (CL31): since 22 Jun 2009 4. Three C-band weather radars in research use
Utö – 59.77° N – 21.37° E – 8 m a.s.l.	Rural island part of the Finnish archipelago, marine climate. Annual average temperature is > 5 °C, wintertime average snow depth is 5–10 cm. Annual rain amount is 900–1100 mm.	1. Doppler lidar: since 25 Apr 2012 2. Ceilometer (CT25K): AWS-cloud base since 15 May 2002
Kuopio Savilahti – 62.89° N – 27.63° E – 190 m a.s.l. Puijo Vehmasmäki	Savilahti: urban site surrounded by lake and forest. Puijo (SMEAR IV): 75 m tower on top of forest covered hill. Vehmasmäki: rural forest site. Climate is continental. Annual average temperature is 3 °C, average wintertime snow depth is 40–60 cm. Annual rain amount is 900–1100 mm.	1. Raman lidar (POLLY^{XT}): continuous measurements since 16 Nov 2012 2. Doppler lidar: since 20 Sep 2011 3. Ceilometer profiles (CT25K): since 7 Dec 2009
Hyytiälä (SMEAR II) – 61.84° N – 24.29° E – 179 m a.s.l.	Rural site surrounded by coniferous forest, continental climate. Annual average temperature is 4 °C, average wintertime snow depth is 40–60 cm. Annual rain amount is 900–1100 mm.	1. Doppler lidar: since 14 Dec 2012 2. Ceilometer (CT25K): profiles since 20 Jun 2009
Sodankylä – 67.37° N – 26.62° E – 171 m a.s.l.	Rural site surrounded by coniferous forest and swamp, subarctic continental climate. Annual average temperature is −2 °C, average wintertime snow depth is 80 cm. Annual rain amount is 300–700 mm.	1. Doppler lidar since Feb 2013 2. Doppler cloud radar (Mira-36S): since 23 May 2012 3. Ceilometer profiles (CT25K): since 20 Jun 2009 4. Microwave radiometers (RPG-2CH-DP, RPG-8CH-DP) since Jan 2013

AMTD
6, 7251–7313, 2013

Table 2. Summary of measured quantities and means of application of each instrument: β and Z_e refer to backscatter coefficient and radar equivalent reflectivity factor, respectively.

Instrument (targets)	Measured parameters	Application
Doppler lidar (aerosol particle, cloud droplets and crystals, snow, precipitation)	Radial profiles of β (co- & cross channels), Doppler velocity, signal-to-noise ratio	Water cloud base height & dynamics, aerosol particle depolarisation ratio and dispersion, mixing layer height, wind profiles, 2–3-D wind field
POLLY^{XT} (aerosol particles, cloud droplets, water vapour)	Vertical profiles of the particle β at 355, 532 & 1064 nm, β at 532 nm (cross polarized) and extinction coefficient at 355 and 532 nm, water vapour at 407 nm	Ångström exponents at 355 and 532 nm & linear/aerosol particle depolarization at 532 nm, particle surface area, volume, effective radius, refractive index and single scattering albedo at 532 nm, water vapour mixing ratio
Cloud radar (cloud droplets & crystals, snow, precipitation & drizzle)	Z_e (co- & cross channels), Doppler velocity, spectral width, signal-to-noise ratio	Cloud top height, cloud vertical dynamics, 3-D cloud image, linear depolarisation ratio
Ceilometer (aerosol particle, cloud droplets and crystals, snow, precipitation)	Vertical profiles of β	Cloud base height, cloudiness, mixing layer height based on aerosol particle distribution
Weather radar (precipitation, snow)	Z, Doppler velocity, Doppler spectral width	Linear depolarisation ratio, precipitation target categorisation, precipitation rate and accumulated amount, wind speed and direction
Sodar (turbulent fluctuations)	Vertical velocity profiles	Shallow (< 400 m) mixing layer depth and wind profile
Microwave radiometer (water vapour)	Brightness temperature	Profiles of temperature and humidity

AMTD
6, 7251–7313, 2013

Table 3. Details of Doppler lidar inter-comparison campaigns and tested parameters.

Time periods	Measurement setup	Tested parameter
	The first inter-comparison period	
2–15 Sep 2011 3 lidars side by side	*Lidars 32, 33, 34:* 1. Focus at infinity 2. Data integration: a. vertical 150 000 pulses per ray, 1 ray per point b. wind 150 000 pulses per ray, 3 rays per point	– Wind profiles every 10 min. – β profiles – β calibration
15–28 Sep 2011 2 lidars side by side	*Lidar 32 & 34:* 1. Focus at infinity 2. Data integration: a. vertical 150 000 pulses per ray, 1 ray per point b. wind 150 000 pulses per ray, 3 rays per point	– Wind profiles every 10 min. – β profiles – β calibration
12 Oct 2011–18 Jan 2012 2 lidars 100 m apart from each other	*Lidar 32:* 1. Focus at infinity 2. Data integration: a. vertical – 150 000 pulses per ray, 1 ray per point until 15 Oct 2011 – 450 000 pulses per ray, 1 ray per point b. Custom scanning (a number of setups) *Lidar 34:* 1. Focus at infinity 2. Data integration: a. vertical – 150 000 pulses per ray, 1 ray per point until 15 Oct 2011 – 450 000 pulses per ray, 1 ray per point b. wind – 150 000 pulses per ray, 3 rays per point until 15 Oct 2011 – 450 000 pulses per ray, 3 rays per point	– β profiles – Testing different integration times – Testing custom scanning strategies
	The second inter-comparison period	
20 Nov 2012–14 Dec 2012 3 lidars side by side, a lidar (nr. 34) 100 m apart	*Lidar 34:* 1. Focus at – 2 km until 23 Nov 2012 – infinite 2. Data integration: a. vertical – 75 000 pulses per ray, 4 rays per point until 23 Nov 2012 – 15 00 pulses per ray, 6 rays per point b. wind – 75 000 pulses per ray, 4 rays per point until 23 Nov 2012 – 15 000 pulses per ray, 4 rays per point c. Custom scanning (a number of setups) *Lidar 46:* 1. Focus at – 2 km until 23 Nov 2012 – infinite until 10 Dec 2012 – 1 km 2. Data integration: a. vertical 15 000 pulses par ray, 6 rays per point b. wind 15 000 pulses per ray, 4 rays per point *Lidar 53:* 1. Focus at – 2 km until 23 Nov 2012 – infinite 2. Data integration: a. vertical 15 000 pulses per ray, 6 rays per point b. wind 15 000 pulses per ray, 4 rays per point *Lidar 54:* 1. Focus at – 2 km until 23 Nov 2012 – infinite until 10 Dec 2012 – 2 km 2. Data integration: a. vertical 15 000 pulses per ray, 6 rays per point b. wind 15 000 pulses per ray, 4 rays per point	– Wind profiles every 3 min. – β profiles – β calibration – Comparing different focus settings

AMTD
6, 7251–7313, 2013

Table 3. Continued.

14 Dec 2012–24 Jan 2013 2 lidars (nr. 53, 54) side by side, a lidar (nr. 34) 100 m apart	*Lidar 34:* 1. Focus at infinite 2. Data integration: a. vertical 15 000 pulses per ray, 6 rays per point b. wind 15 000 pulses per ray, 4 rays per point c. Custom scanning (a number of setups) *Lidar 53:* 1. Focus at infinite 2. Data integration: a. vertical 15 000 pulses per ray, 6 rays per point b. wind 15 000 pulses per ray, 4 rays per point *Lidar 54:* 1. Focus at 2 km 2. Data integration: a. vertical 15 000 pulses per ray, 6 rays per point b. wind 15 000 pulses per ray, 4 rays per point	– Wind profiles every 3 min. – β profiles – β calibration – Comparing different focus settings

AMTD
6, 7251–7313, 2013

Table 4. Dates and times (UTC) of compared example median backscatter coefficient profiles.

	Aerosol particle	Liquid cloud below 1 km	Liquid cloud above 1 km	Ice cloud
First measurement campaign (two left columns in Fig. 5)	8 Sep 2011, at 23:45	12 Sep 2011, at 11:45	8 Sep 2011, at 23:45	4 Sep 2011, at 04:30
Second measurement campaign (two right columns in Fig. 5)	24 Nov 2012, at 15:45	28 Nov 2012, at 20:15	8 Dec 2012, at 14:45	3 Dec 2012, at 04:30
Second measurement campaign (Fig. 6)	12 Dec 2012, at 04:15	11 Dec 2012, at 23:45		10 Dec 2012, at 15:45

AMTD
6, 7251–7313, 2013

Table 5. Statistical comparison of wind speed (a.) and wind direction (b.) measured with Doppler lidars. Shown are number of sample (N), root mean square error (rmse), Pearson correlation (r) and slope of fitted linear curve (k). Half an hour median data of all available range gates presented in Fig. 7 (lidar nos 32–34) and Fig. 8 (lidar nos 34, 46, 53, 54) are included in the respective sample here.

Lidar no	N	k	R	rmse
34 vs. 32	9539	a. 1.00	a. 0.98	a. 1.14
		b. 0.92	b. 0.91	b. 26.40
34 vs. 33	8795	a. 0.99	a. 0.98	a. 1.20
		b. 0.88	b. 0.86	b. 32.70
32 vs. 33	8309	a. 0.98	a. 0.98	a. 1.11
		b. 0.90	b. 0.88	b. 30.28
34 vs. 46	11 440	a. 0.97	a. 0.96	a. 1.60
		b. 0.95	b. 0.96	b. 21.61
34 vs. 53	9908	a. 0.97	a. 0.95	a. 1.80
		b. 0.92	b. 0.95	b. 20.80
34 vs. 54	11 073	a. 0.96	a. 0.96	a. 1.61
		b. 0.93	b. 0.96	b. 19.19
46 vs. 53	10 494	a. 0.94	a. 0.93	a. 2.01
		b. 0.94	b. 0.96	b. 20.83
46 vs. 54	11 773	a. 0.94	a. 0.95	a. 1.80
		b. 0.94	b. 0.96	b. 19.94
53 vs. 54	10 601	a. 0.95	a. 0.96	a. 1.60
		b. 0.95	b. 0.96	b. 18.80

AMTD
6, 7251–7313, 2013

Table 6. Effect of prevailing weather on wind speed measured with DBS technique when comparing observations with sonic anemometer at Puijo tower vs. Doppler lidar at the FMI in Kuopio. Analysis is based on one year of data (20 September 2011–20 September 2012). Bias due to positioning of lidar was removed when investigating bias during rain and snow.

Prevailing conditions	Number of single range gate wind speed values	Slope of linear fitted curve to wind speed data	R^2 for wind speed data	Mean bias in wind direction Lidar-AWS
All	17 494	1.08	0.7	−12.3° (due to inaccurate positioning of lidar)
No precipitation Visibility > 10 000 m	5718	1.13	0.7	–
Fog	1173	1.05	0.7	–
Rain rate	4164	1.06	0.6	–
0.2–0.8 mm h^{-1}	901	1.06	0.655	−1.5°
0.8–2 mm h^{-1}	638	1.07	0.509	−2°
2–5 mm h^{-1}	386	1.07	0.502	−1.6°
> 5 mm h^{-1}	122	1.00	0.358	−1.2°
Snow rate	4388	1.03	0.7	–
0.1–0.2 mm h^{-1}	429	1.02	0.7	−2.4°
0.2–0.5 mm h^{-1}	388	1.02	0.7	−2.6°
> 0.5 mm h^{-1}	338	1.03	0.7	−2.8°

AMTD
6, 7251–7313, 2013

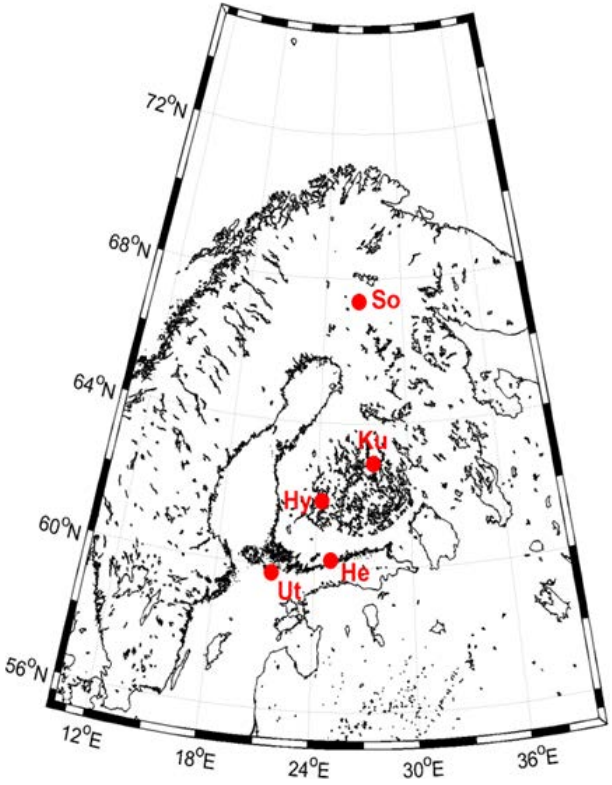

Fig. 1. Map of Finland indicating the network sites: So = Sodankylä, Ku = Kuopio, Hy = Hyytiälä, He = Helsinki and Ut = Utö.

AMTD
6, 7251–7313, 2013

Finland's new ground-based remote-sensing network

A. Hirsikko et al.

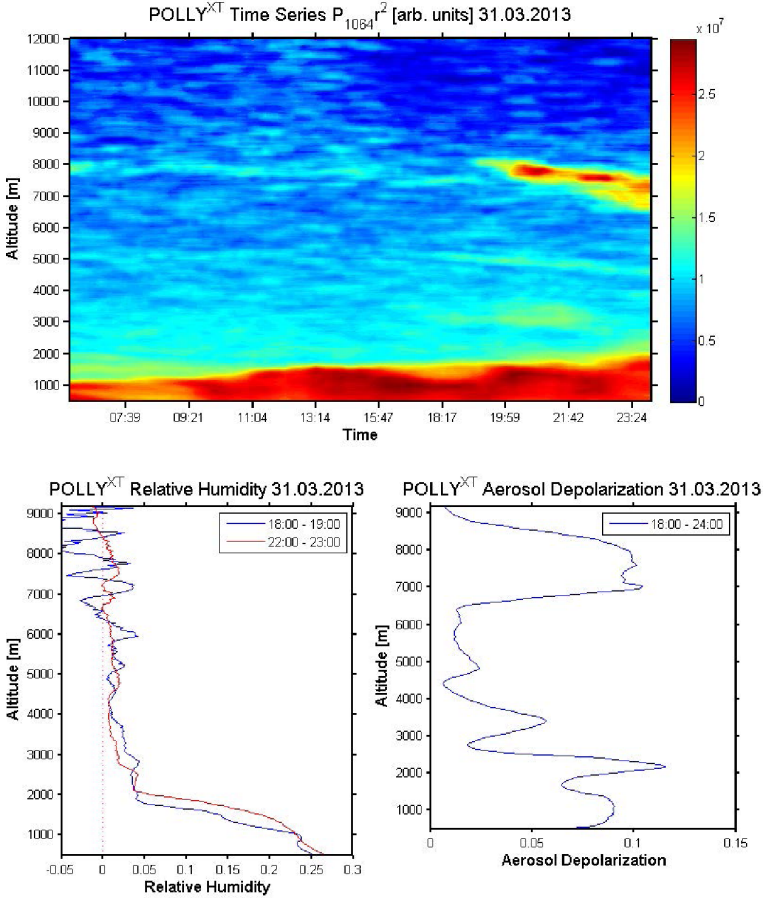

Fig. 2. An example of the range-corrected signal at 1064 nm (on top) of the Polly^{XT} lidar in Vehmasmäki on 31 March 2013. In the left bottom panel one-hour average relative humidity profiles and on the right bottom panel four-hour average depolarisation ratio profile are shown.

AMTD
6, 7251–7313, 2013

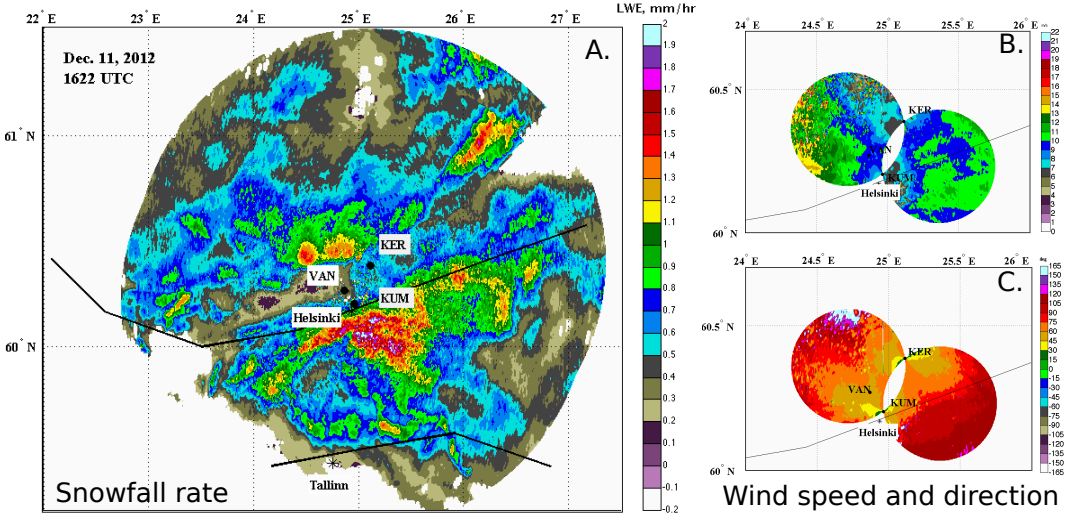

Fig. 3. Helsinki weather radar network observations: **(a)** precipitation (snowfall) rate as measured by the three radars, **(b)**, **(c)** dual-Doppler wind speed and direction estimated from Kumpula and Kerava radar observations.

AMTD
6, 7251–7313, 2013

Finland's new ground-based remote-sensing network

A. Hirsikko et al.

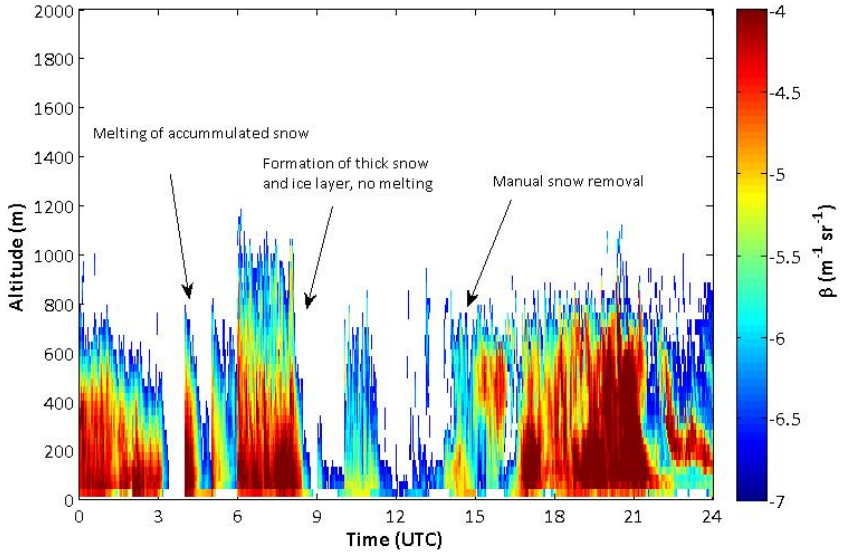

Fig. 4. Effect of snow on Doppler lidar backscattering signal profiles in Helsinki on 4 February 2012.

AMTD
6, 7251–7313, 2013

Finland's new ground-based remote-sensing network

A. Hirsikko et al.

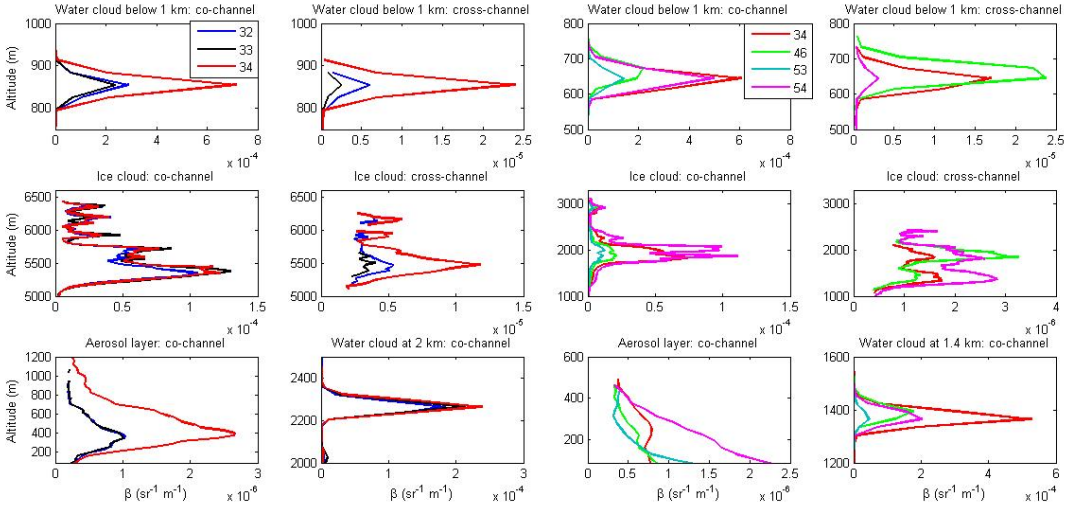

Fig. 5. Half an hour median backscatter coefficient (β) profiles of aerosol particle, water and ice cloud events during the first Doppler lidar inter-comparison campaign (two columns on left hand side) and the second campaign (two columns on right hand side). Shown backscatter coefficient profiles are un-calibrated. The 25 and 75 percentile curves, which were omitted for figure clarity reasons, follow closely the median curves. Telescope focus of each lidar was at infinite. Lidar production numbers are given in the legends.

AMTD
6, 7251–7313, 2013

Finland's new ground-based remote-sensing network

A. Hirsikko et al.

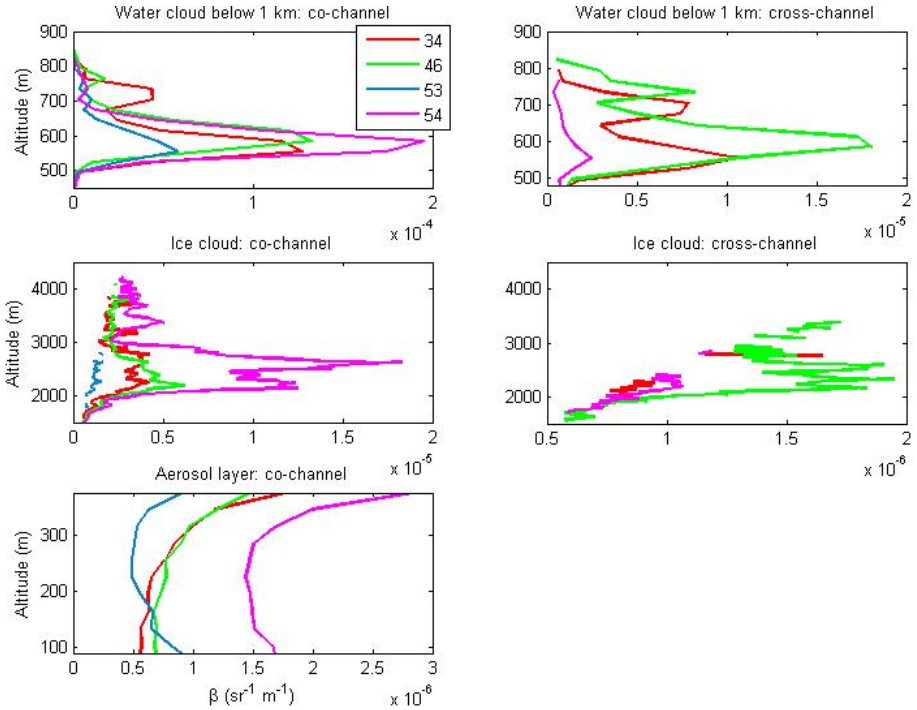

Fig. 6. Half an hour median backscatter coefficient (β) profiles of aerosol particle, water and ice cloud events during the second Doppler lidar inter-comparison campaign. Shown backscatter coefficient profiles are un-calibrated. The 25 and 75 percentile curves follow closely the median and are thus not shown. Lidar production numbers are given in the legend. Telescope focus was set to infinite for lidars 34 and 53, 1 km for lidar 46 and 2 km for lidar 54.

AMTD
6, 7251–7313, 2013

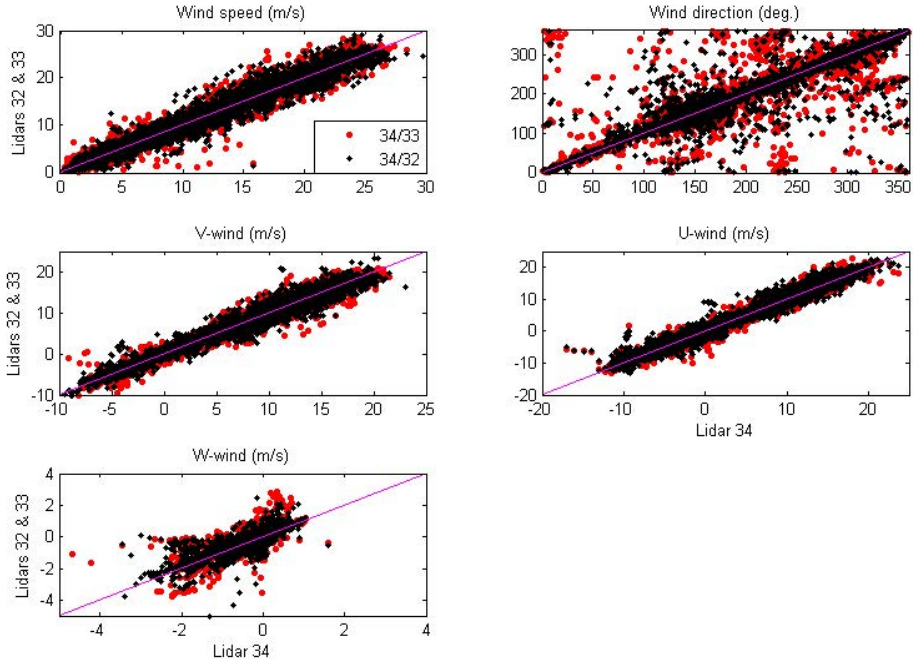

Fig. 7. Horizontal wind speed and direction, and *u*-, *v*- and *w*-components of velocity measured during the first measurement campaign in Helsinki during 2–15 September 2011. Each point is average over half an hour and data from all available range gates are shown. Lidars had similar settings of telescope focus and data integration time.

AMTD
6, 7251–7313, 2013

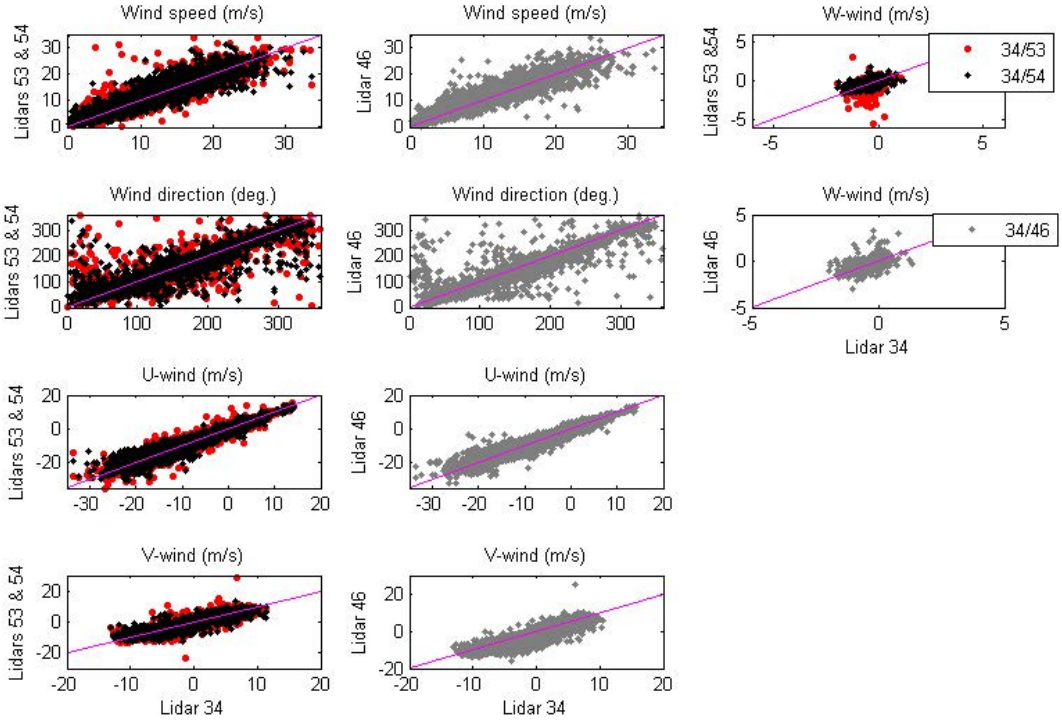

Fig. 8. Horizontal wind speed and direction, and *u*-, *v*- and *w*-components of velocity measured during the first measurement campaign in Helsinki during 24 November–9 December 2012. Each point is average over half an hour and data from all available range gates are shown. Lidars had similar settings of telescope focus and data integration time.

AMTD
6, 7251–7313, 2013

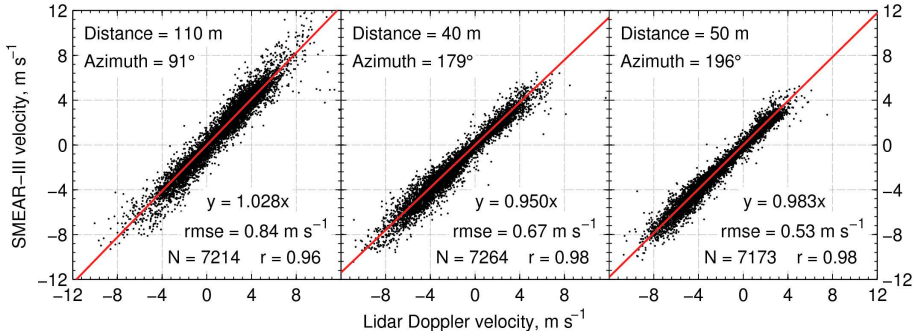

Fig. 9. Comparison of single beam and range gate Doppler velocity with collocated sonic anemometer velocity: Shown are measurements to horizontal separation 110, 40 and 50 m from sonic anemometer, and subsequent statistical parameters are also presented: number of half-an-hour mean velocity sample (*N*), root mean square error (rmse), Pearson correlation (*r*) and slope of fitted linear curve.

AMTD
6, 7251–7313, 2013

Finland's new ground-based remote-sensing network

A. Hirsikko et al.

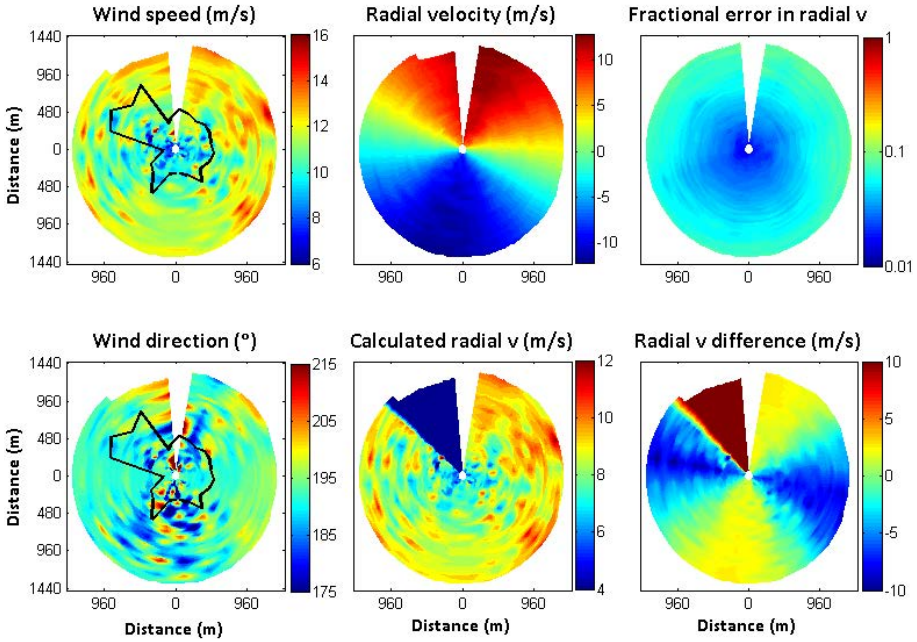

Fig. 10. Example of wind speed (upper left panel) and direction (lower left panel) near surface (with 4° elevation) using Doppler lidar scanning technique at Utö island on 29 September 2012. Black curve is border of the Utö island. A number of small islands on northern and eastern side are not shown. Measured radial velocity (upper middle panel) and its fractional error (upper right panel), calculated radial velocity (lower middle panel) and difference of calculated and absolute value of measured radial velocity (lower right panel) are also shown.

AMTD
6, 7251–7313, 2013

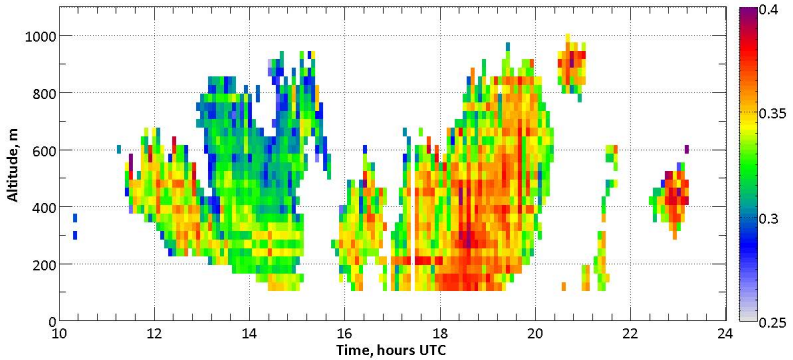

Fig. 11. Depolarisation ratio profiles measured with the Doppler lidar in Utö on 22 May 2012.

AMTD
6, 7251–7313, 2013